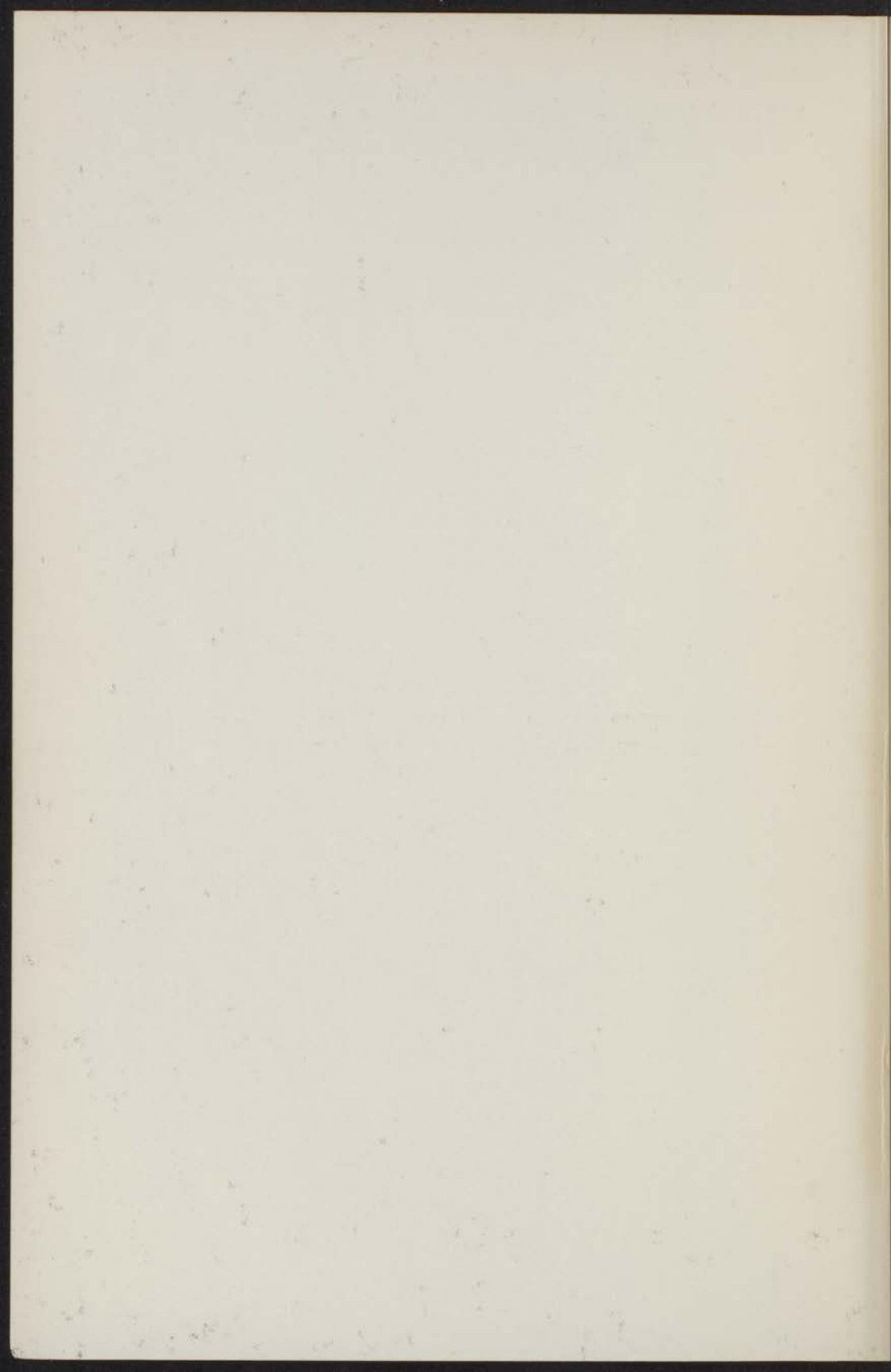


DOUBLE RESONANCE
IN DILUTED
COPPER-TUTTON SALTS

W.Th. WENCKEBACH



DOUBLE RESONANCE IN DILUTED COPPER-TUTTON SALTS

22 OKT. 1970

INSTITUUT-LORENTZ
voor theoretische natuurkunde
Nieuwsteeg 18-Leiden-Nederland

kast dissertaties

DOUBLE RESEARCH IN DILATED COPPER-TITANIUM ZALIN

55 OCT 1970

RESEARCH COMMITTEE
FOR THE STUDY OF
METALLURGICAL RESEARCH

Case Miscellaneous

DOUBLE RESONANCE IN DILUTED COPPER-TUTTON SALTS

PROEFSCHRIFT

TER VERKRIJGING VAN DE GRAAD VAN DOCTOR
IN DE WISKUNDE EN NATUURWETENSCHAPPEN AAN DE
RIJKSUNIVERSITEIT TE LEIDEN,
OP GEZAG VAN DE RECTOR MAGNIFICUS DR. C. SOETEMAN,
HOGLERAAR IN DE FACULTEIT DER LETTEREN,
TEN OVERSTAAN VAN EEN COMMISSIE UIT DE SENAAT
TE VERDEDIGEN OP WOENSDAG 14 OKTOBER 1970
TE KLOKKE 15.15 UUR

DOOR

WILLEM THOMAS WENCKEBACH
GEBOREN TE LEIDEN IN 1943

INSTITUUT-LORENTZ
voor theoretische natuurkunde
Nieuwsteeg 18-Leiden-Nederland

1970

PRINCO NV - ROTTERDAM
THE NETHERLANDS

DOUBLE RESONANCE
IN DILUTED
COPPER-TUTTON SALTS

Promotor: Prof. Dr. Ir. N.J. Poulis

Dit proefschrift is tot stand gekomen

mede in samenwerking met

Dr. T.J.B. Swanenburg

STELLINGEN

I

Meestal wordt bij de theoretische beschrijving van het gedrag van spinsystemen onder invloed van een hoogfrequent wisselveld, in navolging van Provotorov gebruik gemaakt van een coördinatenstelsel, dat roteert met een frequentie gelijk aan die van het genoemde wisselveld. Deze beschrijvingen kunnen op even eenvoudige wijze gegeven worden zonder van zo een roterend coördinatenstelsel gebruik te maken.

Provotorov, B.N. *J. Exptl. Teoret. Fiz.* **41**, 1582 (1961)
Sov. Phys. JETP, **14**, 1126 (1962)

II

De quantummechanische beschrijving van een deeltje in een doos demonstreert op eenvoudige wijze dat de stelling van Von Neumann over de eenduidigheid der Schrödinger-operatoren zijn geldigheid verliest, als men voor de commutatierelaties van deze operatoren de infinitesimale Heisenbergvorm zou gebruiken.

Von Neumann, J., *Math. Ann.* **104**, 570

III

In hoofdstuk II van dit proefschrift werden de voorwaarden geformuleerd waaronder de invoering van het gecombineerde hyperfijn- en dipool-dipoolinteractiesysteem toegestaan is. Deze voorwaarden kunnen experimenteel geverifieerd worden door uitbreiding van de metingen van de polarisatiefactor met experimenten bij grotere microgolfvermogens en hogere temperaturen.

IV

Om de sterkte van de koppeling tussen het dipool-dipoolinteractiesysteem en het kern-Zeeman-systeem te onderzoeken, verdient het aanbeveling om de in dit proefschrift beschreven ENDOR-metingen uit te breiden met experimenten, waarbij grotere overgangswaarschijnlijkheden in het proton-Zeeman-systeem geïnduceerd worden.

V

De wijze waarop Dixon en Walton de resultaten van hun warmtegeleidingsmetingen in $\text{CuK}_2\text{Cl}_4 \cdot 2\text{H}_2\text{O}$ verwerken is aanvechtbaar.

Dixon, G.S., Walton, D., *Phys. Rev.* 185, 735 (1969)

VI

De conclusie van Wittekoek, dat $\text{Cu}(\text{NO}_3)_2 \cdot 3\text{H}_2\text{O}$ de correcte formule is voor het kopernitraat-trihydraat, is onjuist.

Wittekoek, S., proefschrift 1967

VII

Bij paramagnetische zouten, waarvan het E.S.R.-spectrum gedeeltelijk inhomogeen verbreed is, leidt deze inhomogene verbreding in vele gevallen tot een grotere warmtecapaciteit van het dipool-dipoolinteractieterm in de spin-Hamiltoniaan.

VIII

Atsarkin et al. nemen een verandering van de overdracht van de verzadiging van door cross-relaxatie gekoppelde electronspinresonantielijnen in robijn waar, als zij een kernspinresonantielijntje verzadigen. Dit verschijnsel wordt veroorzaakt door hetzelfde mechanisme als het in dit proefschrift beschreven 'distant'-ENDOR-effect.

Atsarkin, V.A., Mefedov, A.E., Rodak, M.I., *Physics Lett.* 27A, 57 (1968)

IX

Uit de wijze waarop Preuss zijn magnetische sperlaag van InSb prepareert valt af te leiden dat een aanzienlijk groter gelijkrichtend vermogen verkregen kan worden, dan door hem bereikt is.

Preuss, E., *Sol. State Electr.* 13, 173 (1970)

X

Bij het ontwerpen van supergeleidende solenoïdes ten behoeve van kernspinresonantie metingen worden veelal numerieke berekeningen uitgevoerd om een zodanige spoelvorm te vinden dat een optimale homogeniteit van het veld verkregen wordt. Het is niet zinvol om bij deze berekeningen homogeniteiten beter dan 10^{-5} cm^{-1} na te streven.

XI

De conclusie van Gill, dat hij bij zijn electronspin-roosterrelaxatietijdmetingen in verdunde koper-Tutton-zouten het Van Vleck-Ramanproces heeft waargenomen is aanvechtbaar.

Gill, J.C., *Proc. Phys. Soc.*, 85, 119 (1965)

XII

Magnetische fasediagrammen van antiferromagnetische eenkristallen kunnen het nauwkeurigst bepaald worden met behulp van magnetische resonantie-methoden.

XIII

De popularisering van de golfsport in Nederland wordt ernstig belemmerd door de vooroordelen die tegen deze sport bestaan. Door op gunstig gelegen plaatsen enige z.g. 'public courses' aan te leggen zouden deze vooroordelen grotendeels uit de weg geruimd kunnen worden.

W. Th. Wenckebach

14 oktober 1970

The first of these is the fact that the...
...of the...
...of the...

The second of these is the fact that the...
...of the...
...of the...

The third of these is the fact that the...
...of the...
...of the...

The fourth of these is the fact that the...
...of the...
...of the...

The fifth of these is the fact that the...
...of the...
...of the...

The sixth of these is the fact that the...
...of the...
...of the...
...of the...
...of the...

The seventh of these is the fact that the...
...of the...
...of the...
...of the...

CONTENTS

CHAPTER I. INTRODUCTION	11
1. Introduction	11
2. THEORY	12
3. THE RISE OF THE THEORY	13
CHAPTER II. THE THEORY OF NUCLEAR DYNAMICS IN FAMILIAR AND UNFAMILIAR REGIONS	15
1. Introduction	15
2. Theoretical description of nuclear dynamic phenomena	17
2.1. The case of a single nucleon in a potential well	17
2.2. The case of a many-nucleon system	20
2.3. The case of a many-nucleon system in a potential well	24
2.4. The case of a many-nucleon system in a potential well	26
3. Theoretical description of nuclear dynamic phenomena	27
3.1. The case of a many-nucleon system in a potential well	27
3.2. The case of a many-nucleon system in a potential well	28
3.3. The case of a many-nucleon system in a potential well	29
3.4. The case of a many-nucleon system in a potential well	30
3.5. The case of a many-nucleon system in a potential well	31
CHAPTER III. THE EXPERIMENTAL ARRANGEMENTS	33
CHAPTER IV. THE EXPERIMENTAL RESULTS OF NUCLEAR DYNAMIC PHENOMENA	35
1. Theoretical description of the dynamic phenomena	35
1.1. The case of a many-nucleon system in a potential well	35
1.2. The case of a many-nucleon system in a potential well	36
2. The theoretical description of the dynamic phenomena	37
2.1. The case of a many-nucleon system in a potential well	37
2.2. The case of a many-nucleon system in a potential well	38
2.3. The case of a many-nucleon system in a potential well	39
3. Conclusion	40

Aan mijn ouders

CONTENTS

CHAPTER I. INTRODUCTION	11
1. Introduction	11
2. The BPPJ theory	13
3. The RSPB theory	17
CHAPTER II. THE THEORY OF NUCLEAR DYNAMIC POLARIZATION AND DISTANT ENDOR	21
1. Introduction	21
2. Theoretical description of nuclear dynamic polarization	21
2.1. The spin Hamiltonian in a rotating frame of reference	21
2.2. Spin temperature	23
2.3. The time dependence of α and β	24
2.4. Proton dynamic polarization	26
3. Theoretical description of distant ENDOR	32
3.1. The equations for distant ENDOR	32
3.2. The solutions of the equations for distant ENDOR	33
3.3. The stationary increment of the E.S.R. signal	34
3.4. The transient behaviour of $J(t)$ after switching on the rf field	37
3.5. The transient behaviour of $J(t)$ after switching off the rf field	40
CHAPTER III. THE EXPERIMENTAL ARRANGEMENT	43
CHAPTER IV. THE EXPERIMENTS OF NUCLEAR DYNAMIC POLARIZATION	49
1. The stationary behaviour of the dynamic polarization	49
1.1. CuKS	49
1.2. $\text{Cu}(\text{NH}_4)\text{S}$, CuRbS, CuCsS	53
2. The transient behaviour of the dynamic polarization	55
2.1. The coefficient $(E_2 - 1)/(E_{st} - 1)$	55
2.2. The time constant τ_1	57
2.3. The time constant τ_2	60
3. Conclusion	62

CHAPTER V. THE EXPERIMENTS OF DISTANT ENDOR	65
1. 1% CuCsS	65
2. 0.5% CuKS and 1% CuRbS	71
3. Conclusion	71
SAMENVATTING	77
CURRICULUM VITAE	79

CONTENTS

11	CHAPTER I. INTRODUCTION
11	1. Introduction
11	2. The EPR theory
11	3. The EPR theory
11	CHAPTER II. THE THEORY OF NUCLEAR DYNAMIC ENDOR
11	1. INTRODUCTION AND DEFINITIONS
11	1. Introduction
11	2. Theoretical description of nuclear dynamic polarization
11	2.1. The spin Hamiltonian in a rotating frame of reference
11	2.1.1. Spin temperature
11	2.1.2. The spin temperature of a unit Q
11	2.1.3. Nuclear dynamic polarization
11	2.1.4. Nuclear dynamic polarization
11	3. Theoretical description of distant ENDOR
11	3.1. The equation for distant ENDOR
11	3.2. The solution of the equation for distant ENDOR
11	3.3. The stationary treatment of the ESR signal
11	3.4. The transient behavior of M_1 after switching on the ν field
11	3.5. The transient behavior of M_2 after switching off the ν field
11	CHAPTER III. THE EXPERIMENTAL ARRANGEMENT
11	CHAPTER IV. THE EXPERIMENTS OF NUCLEAR DYNAMIC ENDOR
11	1. The stationary behavior of the dynamic polarization
11	1.1. CuCsS
11	1.2. CuRbS and CuKS
11	2. The transient behavior of the dynamic polarization
11	2.1. The constant $(\tau_1 - \tau_2)M_1$
11	2.2. The time constant τ_1
11	2.3. The time constant τ_2
11	3. Conclusion

Bedazzled, Cook and Moore (1968)

The experiment was conducted in a laboratory (NOR) by means of the self-experimentation method (NECK) and consisted of a single 60-minute session. A series of 10 trials were run, each one with a different number of trials. In the first trial, only a single trial was run. In the second trial, two trials were run. In the third trial, three trials were run. In the fourth trial, four trials were run. In the fifth trial, five trials were run. In the sixth trial, six trials were run. In the seventh trial, seven trials were run. In the eighth trial, eight trials were run. In the ninth trial, nine trials were run. In the tenth trial, ten trials were run. The results of the experiment are shown in Table 1. The results show that the number of trials run in each session was significantly higher than the number of trials run in the previous session. This suggests that the number of trials run in each session is a function of the number of trials run in the previous session. The results also show that the number of trials run in each session was significantly higher than the number of trials run in the previous session. This suggests that the number of trials run in each session is a function of the number of trials run in the previous session.

The results of the experiment are shown in Table 1. The results show that the number of trials run in each session was significantly higher than the number of trials run in the previous session. This suggests that the number of trials run in each session is a function of the number of trials run in the previous session. The results also show that the number of trials run in each session was significantly higher than the number of trials run in the previous session. This suggests that the number of trials run in each session is a function of the number of trials run in the previous session.

CHAPTER I.

INTRODUCTION.

The Chase, Arthur Penn (1966)

1. Experiments of nuclear dynamic polarization (NDP) by means of the solid state effect and distant ENDOR are carried out in crystals containing electron spins as well as nuclear spins, which are weakly coupled with each other. In these experiments such a crystal is placed in a static magnetic field H_0 . Furthermore a microwave field with a frequency ω in the neighbourhood of the electronic Larmor frequency $\omega_e = \gamma_e H_0$ and an rf field at the nuclear Larmor frequency $\omega_n = \gamma_n H_0$ are directed perpendicular to this static magnetic field. The experimental equipment is arranged in such a way that an electron spin resonance (E.S.R.) signal as well as a nuclear magnetic resonance (N.M.R.) signal can be observed simultaneously. In an experiment of nuclear dynamic polarization a strong microwave field is used to irradiate the sample at a frequency ω while the N.M.R. signal is observed. When this microwave field is switched on an enhancement of the N.M.R. signal is found. Contrary to this, in an experiment of distant ENDOR a strong rf field is applied to saturate the N.M.R. signal, while the E.S.R. signal is observed with a saturating microwave field. In this latter case the application of the rf field results in a considerable change of the E.S.R. signal. These double resonance experiments prove to be a valuable tool to obtain information about spin-spin interactions and the dynamics of spin systems. In the present work such experiments were carried out to study the dynamics of the spin systems in the case of diluted copper Tutton salts*.

A theoretical treatment of nuclear dynamic polarization in diluted paramagnetic salts was given by Jeffries¹. We shall denote this treatment as the BPPJ theory. He considered the polarization to be solely effected by the saturation by the microwave field of 'forbidden' transitions where each time an electron spin and a nuclear spin flip simultaneously. In his description he neglected the influence of the electronic dipole-dipole interaction. In

* For an extensive list of references on nuclear dynamic polarization and distant ENDOR see ref. 1 and 6.

Jeffries's treatment rate equations are used to describe the saturation of the E.S.R. transitions necessary for the dynamic polarization, following the classical treatment of Bloembergen, Purcell and Pound (BPP)². Redfield³ showed, however, that in the case of resonance lines, which are homogeneously broadened as a result of dipole-dipole interaction, the description of BPP could lead to completely wrong results. He gave a correct description of the saturation of homogeneously broadened resonance lines in the case of strongly saturating rf fields. In this description he introduced the concept of a spin temperature in a frame of reference rotating with the frequency of the rf field. His theory was extended to rf fields of arbitrary strength by Provotorov⁴, who separated the dipole-dipole interaction system from the Zeeman systems of the different spin species contained in the sample. Each of these systems was assumed to have its own spin temperature. Solomon⁵ suggested that a description of nuclear dynamic polarization should be based on these new descriptions of saturated resonance signals. Abragam and Borghini⁶ gave such a description (the RSPB theory). They used three spin temperatures: one for the electron Zeeman system, one for the nuclear Zeeman system and one for the dipole-dipole interaction system. In the case of a strong electronic dipole-dipole interaction the RSPB theory gives completely different results from those resulting from the theory of Jeffries¹. In the case of a very small electronic dipole-dipole interaction the results of both theories are the same, however. Experiments of NDP in $\text{La}_2\text{Mg}_3(\text{NO}_3)_{12} \cdot 24\text{H}_2\text{O}$ with Nd and Ce as paramagnetic impurities could be explained by the RSPB theory⁷.

A theoretical treatment of distant ENDOR was also given by Jeffries¹. A more elaborate description in the case of inhomogeneously broadened E.S.R. lines was given by Lambe et al.⁸. In both treatments the distant ENDOR effect is considered to be effected by the saturation of forbidden transitions only. In neither of these two descriptions the electronic dipole-dipole interaction system is accounted for.

Recently a very strong coupling between the dipole-dipole interaction system and the nuclear Zeeman system as used in the RSPB theory has experimentally been proven to exist at liquid Helium temperatures and a static magnetic field of about 3 kG⁹. Experimental evidence of this strong coupling was also obtained by other authors¹⁰. As a result of this evidence a simplified description can be given of the spin dynamics of a crystal containing electron spins and nuclear spins. In this description only two spin systems remain: the electron Zeeman system and the combined dipole-dipole interaction and nuclear Zeeman system. Hence only two spin temperatures are used, one for each of these systems, instead of the three spin temperatures used by Abragam and Borghini. This strong coupling between the dipole-dipole interaction system and the nuclear Zeeman system yields an extra mechanism besides those of the RSPB theory for nuclear dynamic polarization as well as distant ENDOR. Both effects are then effected by saturating the allowed E.S.R. transitions instead of the forbidden ones. In this work

double resonance experiments in copper Tutton salts diluted with Zinc, where this strong coupling between the dipole-dipole interaction system and the nuclear Zeeman system can be expected, will be discussed. In the next two sections the main characteristics of the theory of Jeffries and the RSPB theory will be reviewed. These theories will be illustrated by calculating the stationary behaviour of the proton dynamic polarization in a diluted copper Tutton salt. In fig. 1.5 at the end of this chapter the results of these calculations will be given. In chapter II the new theory of dynamic polarization and distant ENDOR will be treated. The stationary behaviour of the proton dynamic polarization according to this new theory will also be given in fig. 1.5. In the succeeding chapters the experiments on these salts and their results will be presented and compared with this new theory.

2. *The BPPJ theory.* Jeffries treated the behaviour of nuclear dynamic polarization in diluted paramagnetic salts containing one electron spin species and one nuclear spin species. In his treatment he neglected the electronic dipole-dipole interaction. Hence he considered the electron spins as isolated from each other, interacting with neighbouring nuclear spins only. The spin Hamiltonian can then be written as:

$$\mathcal{H}_{\text{spin}} = \mathcal{H}_e + \mathcal{H}_n + \mathcal{H}_{SI} \quad (1.1)$$

Here the first two terms are the Zeeman energies of the electron spin S and the nuclear spin I in the static magnetic field H_0 . Their resonance frequencies in this static magnetic field are ω_e and ω_n respectively. \mathcal{H}_{SI} , the electron-nuclear dipole-dipole interaction is considered to be at least one order of magnitude smaller than the first two terms of the spin Hamiltonian.

A simple approach to the problem is obtained by considering a number of pairs consisting of only one electron spin $S = \frac{1}{2}$ and only one nuclear spin $I = \frac{1}{2}$. The dipolar interaction term \mathcal{H}_{SI} of the spins in such a pair is

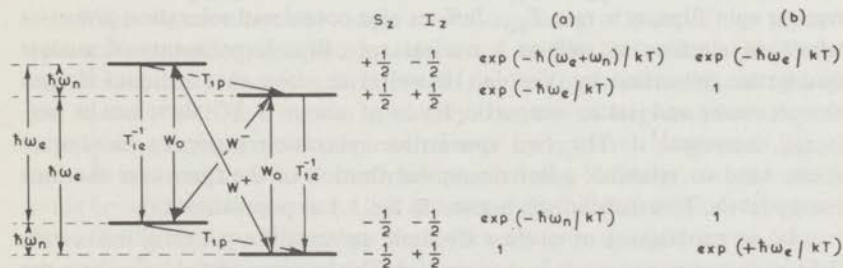


Fig. 1.1. Energy levels of a simple pair of an electron spin and a nuclear spin. It should be noted that the electronic and nuclear magnetic moments are considered to have opposite signs. (a) represents the thermal equilibrium population of the energy levels. (b) represents the population of the levels, when the transitions $\Delta S_z = \pm 1$, $\Delta I_z = \pm 1$ are strongly saturated by a microwave field at frequency $\omega_e - \omega_n$.

considered to be a weak perturbation on the Zeeman terms in the spin Hamiltonian. Then the zero order energy levels of this system are simply the Zeeman levels. They are denoted in fig. 1.1 by the eigenvalues of S_z and I_z . When a microwave field perpendicular to the static magnetic field, with a frequency $\omega = \omega_e$, is applied, transitions of the type $\Delta S_z = \pm 1, \Delta I_z = 0$ will be induced with a rate W_0 . In this zero order approximation transitions of the type $\Delta S_z = \pm 1, \Delta I_z = \pm 1$ and $\Delta S_z = \pm 1, \Delta I_z = \mp 1$ are completely forbidden. When the dipole-dipole interaction between S and I is taken into account, however, finite probabilities W^- and W^+ respectively for these two 'forbidden' transitions are found. These probabilities W^- and W^+ are about H_{10c}^2/H_0^2 smaller than W_0 , where H_{10c} is the local field of S at the location of I . The 'forbidden' transitions are observed at microwave frequencies $\omega = \omega_e - \omega_n$ and $\omega = \omega_e + \omega_n$. The microwave absorption signal owing to the three transitions is given in fig. 1.2.

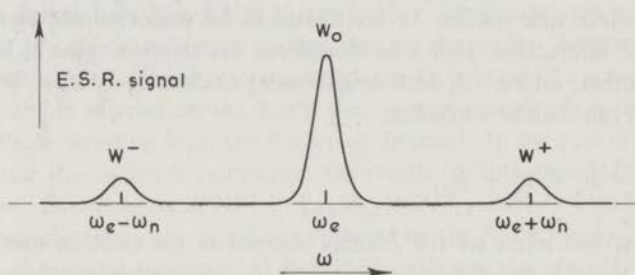


Fig. 1.2. The microwave absorption signal of a simple pair consisting of one electron spin $S = \frac{1}{2}$ and one nuclear spin $I = \frac{1}{2}$.

Beside the induced transitions there are two important spin-lattice relaxation processes: the electron spin-lattice relaxation, where only an electron spin flips, at a rate T_{1e}^{-1} and the nuclear spin-lattice relaxation where only a nuclear spin flips, at a rate T_{1n}^{-1} . Jeffries also considered relaxation processes where an electron as well as a nuclear spin flip. Experiments of nuclear spin-lattice relaxation by Van den Heuvel et al. show that at liquid Helium temperatures and static magnetic fields of about 3 kG these can be neglected, however¹¹. The two spin-lattice relaxation processes mentioned above tend to establish a Boltzmann distribution of the spins over the four energy levels. This distribution is given in fig. 1.1 as population (a).

In an experiment of nuclear dynamic polarization a strong microwave field at frequency $\omega = \omega_e - \omega_n$ is applied. This microwave field equalizes the populations of the states $|S_z, I_z\rangle = |-\frac{1}{2}, -\frac{1}{2}\rangle$ and $|+\frac{1}{2}, +\frac{1}{2}\rangle$. On the other hand the electron spin-lattice relaxation will tend to establish the thermal equilibrium distribution with a Boltzmann factor $\exp(-\hbar\omega_e/kT)$ between the levels $|-\frac{1}{2}, -\frac{1}{2}\rangle$ and $|+\frac{1}{2}, -\frac{1}{2}\rangle$ as well as between the levels $|-\frac{1}{2}, +\frac{1}{2}\rangle$ and

$|+\frac{1}{2}, +\frac{1}{2}\rangle$. The distribution which results when the nuclear spin-lattice relaxation is neglected is given in fig. 1.1 by population (b).

We will define the electron spin polarization P and the nuclear spin polarization p by:

$$P = \frac{N_e^- - N_e^+}{N_e^+ + N_e^-} \quad \text{and} \quad p = \frac{N_n^+ - N_n^-}{N_n^+ + N_n^-} \quad (1.2)$$

where N_e^\pm is the number of electron spins for which $S_z = \pm\frac{1}{2}$ and N_n^\pm is the number of nuclear spins for which $I_z = \pm\frac{1}{2}$. It should be noted that the magnitude of the N.M.R. signal is proportional to p . When no microwave field is present, the populations of the energy levels will be those given by (a) in fig. 1.1, and the polarizations will be given by:

$$P = P_o = \tanh \frac{\hbar\omega_e}{kT_L} \quad \text{and} \quad p = p_o = \tanh \frac{\hbar\omega_n}{kT_L} \quad (1.3)$$

where T_L is the lattice temperature. When the microwave field at frequency $\omega = \omega_e - \omega_n$ is applied, the populations of the energy levels will change and will be given by (b) in fig. 1.1. Then the new equilibrium polarization of both spin species will be equal and given by:

$$p = P = P_o = \tanh \frac{\hbar\omega_e}{kT_L} \quad (1.4)$$

Thus the nuclear polarization and hence the magnitude of the N.M.R. signal is enhanced by a factor: $E = p/p_o = P_o/p_o$. Under our experimental conditions ($H_o = 3$ kG, $T \geq 1$ K) this enhancement is approximately given by $E \cong \omega_e/\omega_n$.

Similarly when a strong microwave field with a frequency $\omega = \omega_e + \omega_n$ is applied the nuclear polarization and hence the N.M.R. signal is enhanced by a factor $E \cong \omega_e/\omega_n$. The N.M.R. signal then becomes an emission signal.

When we abandon our simple model consisting of pairs of one electron spin and one nuclear spin and consider a real sample, like a diluted Cu-Tutton salt, we encounter two complications. In the first place each electron spin will not interact with one nuclear spin only, but with a large number of nuclei surrounding it. Hence the simple scheme of energy levels as given in fig. 1.1 must be replaced by a much more complicated one. Secondly, owing to the dipolar broadening, the resonance line and its two 'forbidden' satellites as shown in fig. 1.2 will overlap. This means that when a microwave field with a frequency ω in the neighbourhood of ω_e is applied, all three transition probabilities W_o , W^+ and W^- will be induced. When these two complications and spin-lattice relaxation are taken into account, rate equations can be formed for the time behaviour of the electron spin polarization P and the nuclear spin polarization p :

$$\frac{dp}{dt} = W^-(p - P) - W^+(p + P) - (p - p_0) \frac{1}{T_{1n}} \quad (1.5a)$$

$$\frac{dP_e}{dt} = -W_0 P + \frac{N_n}{N_e} W^-(p - P) - \frac{N_n}{N_e} W^+(p + P) - (P - P_0) \frac{1}{T_{1e}} \quad (1.5b)$$

In these equations W^\pm is defined as the probability that a nuclear spin flips owing to a 'forbidden' transition. Since each electron spin interacts with on the average N_n/N_e nuclear spins, an electron spin will have to flip an average of N_n/N_e times, owing to forbidden transitions, to make a particular nuclear spin flip. Hence the probability that an electron spin will flip owing to a forbidden transition is $(N_n/N_e)W^\pm$.

In the experiments described in chapter IV a single crystal of diluted Cu-Tutton salt is directed with its b-axis parallel to a static magnetic field H_0 of about 3 kG. Then from the eqs. (1.5a) and (1.5b) the stationary enhancement E_{st} of the nuclear polarization can be approximated by:

$$E_{st} = \frac{W_0 T_{1e} - (\omega_e/\omega_n)(W^+ - W^-) T_{1n}}{W_0 T_{1e}(W^+ T_{1n} + W^- T_{1n} + 1) - f(W^+ T_{1n} - W^- T_{1n})^2} \quad (1.6)$$

where $f = N_n T_{1e}/N_e T_{1n}$. In fig. 1.5 at the end of this chapter, curve I represents E_{st} as a function of $s.g(\Delta) \equiv W_0 T_{1e}$ according to eq.(1.6) in the case of $Zn(NH_4)_2(SO_4)_2 \cdot 6H_2O$ containing 1% Cu^{2+} ions for $\Delta \equiv \omega_e - \omega = 370$ MHz (see fig. 1.3). For T_{1e} and T_{1p} experimental values are used. W^+

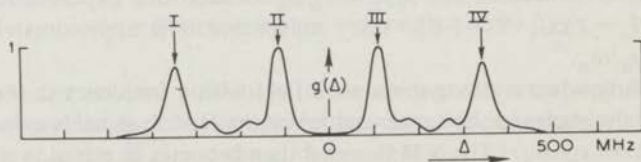


Fig. 1.3. The E.S.R. line shape function $g(\Delta)$ in the case of $Zn(NH_4)_2(SO_4)_2 \cdot 6H_2O$ containing 1% Cu^{2+} ions for $H = 3$ kG and parallel to the crystal b-axis and for $T = 4.2$ K.

and W^- were estimated by a rough method to calculate H_{10c}^2/H_0^2 given by Jeffries, to be about $10^{-6} W_0$. To obtain this estimate, X-ray diffraction data for Tutton salts¹² were used to obtain the distance between the copper ion and its nearest protons, which is necessary for the calculation of H_{10c} . It can be seen from fig. 1.5 curve I that no enhancement of the proton polarization can be expected. This result of the BPPJ theory can also be deduced in the following simple manner from the eqs.(1.5a) and (1.5b):

From eq.(1.5a) can be seen that there are several competing processes determining the equilibrium value of the proton polarization p . In the first place the spin-lattice relaxation, which tends to make p equal to p_o at a rate T_{1n}^{-1} . Secondly the two types of forbidden transitions, tending to make p equal to $+P$ (the electron spin polarization) or $-P$, both of which different from p_o , with a transition probability W^- and W^+ respectively. When we want to obtain an appreciable change of the proton polarization p from its thermal equilibrium value p_o , we must see to it that the probability of one of the forbidden transitions is of the same order of magnitude or larger than the proton spin-lattice relaxation rate, hence W^+T_{1n} or $W^-T_{1n} \gtrsim 1$. On the other hand the electron spin polarization P is mainly determined by the term W_oP and the electron spin-lattice relaxation term in eq.(1.5b). It follows that if W_oT_{1e} is of the order 1 or higher, P decreases owing to saturation of the E.S.R. signal. Now W^+/W_o and W^-/W_o were estimated to be of the order 10^{-6} for $\Delta = 370$ MHz, while T_{1e} and T_{1n} were measured to be of the same order of magnitude¹¹. Then W_oT_{1e} has to be of the order 10^6 to satisfy the condition W^+T_{1n} or $W^-T_{1n} \cong 1$. At such a large value of W_oT_{1e} , P will even be lower than p_o however, and hence the proton polarization $|p|$ will diminish instead of increase owing to the forbidden transitions.

3. *The RSPB theory.* Abragam and Borghini, like Jeffries, treated the behaviour of nuclear dynamic polarization in diluted paramagnetic salts containing one electron spin species and one nuclear spin species. Unlike Jeffries however, they did not neglect the electronic dipole-dipole interaction. The spin Hamiltonian can then be written as:

$$\mathcal{H}_{\text{spin}} = \mathcal{H}_e + \mathcal{H}_n + \mathcal{H}_{\text{int}} \quad (1.7)$$

Here \mathcal{H}_{int} contains all spin-spin interactions. In Abragam and Borghini's description the dynamic polarization is effected, as in Jeffries's description, by saturating forbidden transitions with a microwave field with a frequency ω in the neighbourhood of the Larmor frequency of the electron spins ω_e . Following Provotorov they introduced a frame of reference rotating with the microwave frequency about the direction of H_o . In this rotating frame the spin system can be described as consisting of three parts, each in internal quasi-equilibrium. They are the electron Zeeman system, originating in the term \mathcal{H}_e of the Hamiltonian, with the spin temperature $T_e = 1/k\alpha$, the nuclear Zeeman system, originating in the term \mathcal{H}_n of the Hamiltonian, with the spin temperature $T_n = 1/k\beta$ and the interaction system, originating in the term \mathcal{H}_{int} of the Hamiltonian, with the spin temperature $T_{\text{int}} = 1/k\gamma$.

Abragam and Borghini gave equations for the time dependence of α , β and γ owing to the microwave field and spin-lattice relaxation. They, however, neglected several terms in these equations, which are not negligible in the case of diluted Cu-Tutton salts. A complete set of equations for the time dependence of α , β and γ was derived by Theobald¹³:

$$\begin{aligned} \Delta^2 \frac{\partial \alpha}{\partial t} = & -\Delta^2 W_0(\alpha - \gamma) - \frac{N_n}{N_e} W^+ \Delta (\alpha \Delta - (\Delta + \omega_n) \gamma + \beta \omega_n) + \\ & - \frac{N_n}{N_e} W^- \Delta (\alpha \Delta - (\Delta - \omega_n) \gamma - \beta \omega_n) + \\ & - \Delta^2 \frac{1}{T_{1e}} \left(\alpha - \frac{\omega_e}{\Delta} \beta_L \right) \end{aligned} \quad (1.8a)$$

$$\begin{aligned} \omega_{\text{int}}^2 \frac{\partial \gamma}{\partial t} = & +\Delta^2 W_0(\alpha - \gamma) + \frac{N_n}{N_e} W^+ (\Delta + \omega_n) (\alpha \Delta - (\Delta + \omega_n) \gamma + \beta \omega_n) + \\ & + \frac{N_n}{N_e} W^- (\Delta - \omega_n) (\alpha \Delta - (\Delta - \omega_n) \gamma - \beta \omega_n) + \\ & - \omega_{\text{int}}^2 \frac{1}{T_{\text{int}}} (\gamma - \beta_L) \end{aligned} \quad (1.8b)$$

$$\begin{aligned} \omega_n^2 \frac{\partial \beta}{\partial t} = & -W^+ \omega_n (\alpha \Delta - (\Delta + \omega_n) \gamma + \beta \omega_n) + \\ & + W^- \omega_n (\alpha \Delta - (\Delta - \omega_n) \gamma - \beta \omega_n) + \\ & - \omega_n^2 \frac{1}{T_{1n}} (\beta - \beta_L) \end{aligned} \quad (1.8c)$$

where $\Delta = \omega_e - \omega$, $T_L = 1/k\beta_L$ is the lattice temperature and T_{int} the spin-lattice relaxation time of the interaction system. Furthermore ω_{int} is defined

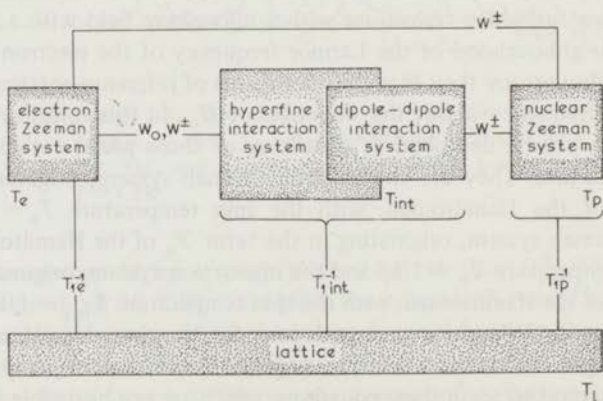


Fig. 1.4. Block diagram of the spin systems in the case of a diluted Cu-Tutton salt, according to the RSPB theory.

by the equation:

$$\text{Tr} (\mathcal{H}_{\text{int}})^2 = \frac{1}{4} N_e \hbar^2 \omega_{\text{int}}^2 \quad (1.9)$$

In fig. 1.4 the spin systems and the lattice in the case of a Cu-Tutton salt are shown as a block diagram. It should be noted that in this case \mathcal{H}_{int} is greatly enlarged by the hyperfine interaction term owing to the hyperfine interaction of the nuclear spin and the electron spin of the Cu^{2+} ion. The energy transports owing to the microwave field and spin-lattice relaxation are denoted by arrows in fig. 1.4.

From the equations (1.8a), (1.8b) and (1.8c) the stationary solutions of α , β and γ can be obtained. Because in the high temperature limit p is proportional to the inverse spin temperature β , the stationary enhancement, E_{st} , can also be calculated. In the case of a crystal of diluted Cu-Tutton salt directed with its b-axis parallel to a static magnetic field of about 3 kG and T between 1 and 4 K, E_{st} can be approximated by:

$$E_{\text{st}} = \frac{\beta_{\text{st}}}{\beta_{\text{L}}} = \frac{\omega_e \Delta + \frac{T_{1e}}{T_{1\text{int}}} \omega_{\text{int}}^2 + \frac{T_{1e} N_n}{T_{1n} N_e} \omega_n^2 + (\Delta^2 + \frac{T_{1e}}{T_{1\text{int}}} \omega_{\text{int}}^2) \frac{1}{(W^+ + W^-) T_{1n}}}{\Delta^2 + \frac{T_{1e}}{T_{1\text{int}}} \omega_{\text{int}}^2 + \frac{T_{1e} N_n}{T_{1n} N_e} \omega_n^2 + (\Delta^2 + \frac{T_{1e}}{T_{1\text{int}}} \omega_{\text{int}}^2) \frac{1}{(W^+ + W^-) T_{1n}}} \quad (1.10)$$

Because \mathcal{H}_{int} is mainly determined by the hyperfine interaction term of the

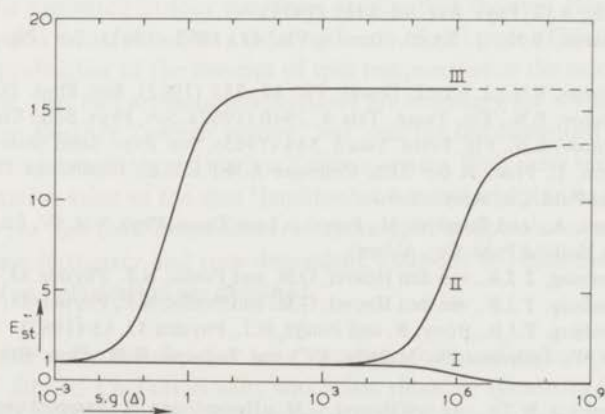


Fig. 1.5. E_{st} as a function of $s.g.(\Delta)$ in the case of $\text{Zn}(\text{NH}_4)_2(\text{SO}_4)_2 \cdot 6\text{H}_2\text{O}$ containing 1% Cu^{2+} ions for $\Delta = 370$ MHz: Curve I: according to the BPPJ theory, curve II: according to the RSPB theory, curve III: according to the theory presented in chapter II.

electron spin S and the nuclear spin I' , of the Copper ion, we may approximate $\omega_{\text{int}}^2 = \frac{5}{4}A_z^2$. Here A_z originates in the term $\hbar A_z S_z I_z$ of the hyperfine interaction. In fig. 1.5 curve II E_{st} is plotted as a function of $W_0(\Delta)T_{1e} = s.g(\Delta)$ in the case of $\text{Zn}(\text{NH}_4)_2(\text{SO}_4)_2 \cdot 6\text{H}_2\text{O}$ containing 1% Cu, for $\Delta = \omega_e - \omega = 370$ MHz and a static magnetic field of 3 kG. To obtain curve II eq.(1.10) is used. In this figure the results in the case of the BPPJ theory are presented by curve I, and the results in the case of the new theory, presented in chapter II, are given by curve III. To obtain curve II, the same values for T_{1e} , T_{1n} , W^+ and W^- are used as in the case of the BPPJ theory. The spin-lattice relaxation of the interaction system is supposed to be mainly due to the electronic spin-lattice relaxation, hence $T_{1\text{int}} = T_{1e}$. It can be seen from fig. 1.5 curve II that an enhancement is observed when $(W^+ + W^-)T_{1n}$ is of the order 1, and hence $s.g(\Delta)$ is of the order 10^6 .

REFERENCES

1. Leifson, O.S. and Jeffries, C.D., Phys. Rev. **122**, 1781 (1961).
Schmugge, J.T. and Jeffries, C.D., Phys. Rev. **138**, A 1785 (1965).
Jeffries, C.D., Dynamic Nuclear Orientation, Interscience Publ., John Wiley & Sons, New York.
2. Bloembergen, N., Purcell, E.M. and Pound, R.V., Phys. Rev. **73**, 670 (1948).
3. Redfield, A.G., Phys. Rev. **98**, 1787 (1955).
4. Provotorov, B.N., J. Exptl. Teoret. Fiz. **41**, 1582 (1961), Sov. Phys. JETP **14**, 1126.
Provotorov, B.N., J. Exptl. Teoret. Fiz. **42**, 882 (1962), Sov. Phys. JETP **15**, 611.
Provotorov, B.N., Fiz. Tverd. Tela **4**, 2940 (1962), Sov. Phys. Solid State, **4**, 2155.
Provotorov, B.N., Fiz. Tverd. Tela **5**, 564 (1963), Sov. Phys. Solid State **5**, 411.
5. Solomon, I., Proc. of the XIth. Colloque A.M.P.E.R.E., Eindhoven 1962. (North Holland Publ. Co., Amsterdam).
6. Abragam, A., and Borghini, M., Progr. in Low Temp. Phys. Vol. IV, Ed. C.J. Gorter (North Holland Publ. Co., A'dam).
7. Swanenburg, T.J.B., van den Heuvel, G.M. and Poulis, N.J., Physica **33**, 707 (1967).
Swanenburg, T.J.B., van den Heuvel, G.M. and Poulis, N.J., Physica **35**, 369 (1967).
Swanenburg, T.J.B., Booy, R. and Poulis, N.J., Physica **37**, 65 (1967).
8. Lambe, J., Laurence, N., McIrvine, E.C. and Terhune, R.W., Phys. Rev. **122**, 1161 (1961).
9. Wenckebach, W.Th., van den Heuvel, G.M., Hoogstraate, H., Swanenburg, T.J.B., and Poulis, N.J., Phys. Rev. Lett. **22**, 581 (1969).
10. Atsarkin, V.A., and Rodak, M.I., Fizika Tverd. Tela **11**, 613 (1969). Sov. Phys. Solid State **11**, 493.
11. Van den Heuvel, G.M. and Poulis, N.J., Physica, to be published.
12. Montgomery, H., Lingafelder, E.C., Acta Cryst. **17**, 1295 (1964).
13. Theobald, G., Compt. Rend. Acad. Science. Paris, **t 268**, B 529 (1969).

CHAPTER II
THE THEORY OF
NUCLEAR DYNAMIC POLARIZATION
AND DISTANT ENDOR.

The Knack, Richard Lester (1965)

1. In chapter I two theoretical treatments of nuclear dynamic polarization were reviewed: The BPPJ theory and the RSPB theory. It was pointed out in chapter I that in neither of the two treatments the strong coupling between the spin-spin interaction system and the nuclear Zeeman system was supposed to exist. In the present chapter a new theory of nuclear dynamic polarization will be presented in which this strong coupling is taken into account. In a second part of this chapter, this theory will be extended to the case of distant ENDOR.

2. *Theoretical description of nuclear dynamic polarization.* The theoretical description of the dynamic polarization of the protons in Cu-Tutton salts will be presented in four successive stages: first the spin Hamiltonian is presented, and transformed to a rotating frame of reference. This is necessary for the introduction of the concept of spin temperature in the next step. It is pointed out, that two separate temperatures are necessary for the description: one for the electron Zeeman system, and one for the combined hyperfine, dipole-dipole interaction, and nuclear Zeeman system. With these temperatures the expectation value of the spin Hamiltonian is calculated. In the third stage, equations for the time dependence of these spin temperatures are derived. Finally their stationary and time-dependent solutions and thus the behaviour of the proton polarization are obtained.

2.1. *The spin Hamiltonian in a rotating frame of reference.* A single crystal of diluted Cu-Tutton salt, which has rhombic symmetry, is directed with one of its rhombic axes parallel to a static magnetic field. The z axis of the laboratory frame of reference is chosen parallel to this static magnetic field. Finally a microwave field with a frequency ω in the neighbourhood of the electron spin resonance frequency ω_e of the Cu ion is directed parallel to the x axis of the frame of reference. The spin Hamiltonian can then be

written as¹:

$$\mathcal{H}_{\text{spin}} = \hbar\omega_e S_z + \hbar\omega_p I_z + \frac{1}{2}\hbar\omega_1\{S^+ e^{i\omega t} + S^- e^{-i\omega t}\} + \\ + \hbar\{A_z S_z I'_z + A_x S_x I'_x + A_y S_y I'_y\} + \mathcal{H}_D.$$

Here the first two terms are the Zeeman energies of the total electron spin S and the total proton spin I in the static magnetic field H_0 . Their resonance frequencies in this static magnetic field are ω_e and ω_p respectively. The microwave field, which has the amplitude $H_1 = \hbar\omega_1/\gamma_e$ yields the term $\frac{1}{2}\hbar\omega_1\{S^+ \exp(i\omega t) + S^- \exp(-i\omega t)\}$, where $S^\pm = S_x \pm iS_y$. The fourth term is the hyperfine interaction of the electron spins S with the nuclear spins I' of the copper ions. All the remaining spin-spin interactions are taken together in the last term of the Hamiltonian. Finally the nuclear quadrupole interaction of the copper ions in the electric crystal field and the Zeeman term of the Cu nuclei are neglected because they are an order of magnitude smaller than the hyperfine interaction of S and I' .

In order to be able to introduce the concept of spin temperature in the presence of a strong microwave field, as will be done below, it is necessary to transform to a rotating frame of reference². This transformation is carried out with the unitary operator

$$U = \exp(i\omega S_z t)$$

which transforms the Hamiltonian as follows:

$$\mathcal{H}'_{\text{spin}} = \hbar\Delta S_z + \hbar\omega_p I_z + \frac{1}{2}\hbar\omega_1\{S^+ + S^-\} + \hbar A_z S_z I'_z + \\ + \mathcal{H}'_D + \sum_{\substack{m=-2 \\ m \neq 0}}^{m=+2} B_m e^{im\omega t},$$

where $\Delta = \omega_e - \omega$, \mathcal{H}'_D is the secular part of \mathcal{H}_D , and the last terms, which are non-secular and oscillate rapidly, originate in $\hbar(A_x S_x I'_x + A_y S_y I'_y)$ and the non-secular part of \mathcal{H}_D . As $|\Delta|$ is much smaller than ω , these last terms which oscillate with a frequency ω or 2ω cannot cause transitions, hence they can be neglected³. Then the spin Hamiltonian in a rotating frame of reference is reduced to:

$$\mathcal{H}'_{\text{spin}} = \hbar\Delta S_z + \frac{1}{2}\hbar\omega_1(S^+ + S^-) + \mathcal{H}^0, \quad (2.1)$$

where

$$\mathcal{H}^0 = \hbar A_z S_z I'_z + \hbar\omega_p I_z + \mathcal{H}'_D.$$

2.2. *Spin temperature.* The secular part of the spin Hamiltonian (2.1) in the rotating frame of reference can be considered as consisting of two parts, $\hbar\Delta S_z$ and \mathcal{H}^0 , each describing a spin system in internal equilibrium. Then these spin systems may have different spin temperatures. A number of processes is known, which tend to establish this equilibrium within each of these systems: the cross relaxation, which makes possible a rapid exchange of hyperfine energy $\hbar A_z S_z I_z'$ and interaction energy \mathcal{H}'_D , furthermore a fast exchange of proton Zeeman energy and dipole-dipole interaction energy has been proven to exist⁴ and finally spin diffusion ensures a homogeneous temperature in both systems.

On the other hand two processes tend to destroy the internal equilibrium in the two systems: the transitions caused by the microwave field and the spin-lattice relaxation.

At liquid helium temperatures and in the presence of not too strong microwave fields, the time constants involved in the process of microwave induced transitions and spin-lattice relaxation are several orders of magnitude larger than those involved in cross relaxation, exchange of dipole-dipole interaction energy and nuclear Zeeman energy, and those of spin diffusion. So a description with two separate systems in internal quasi-equilibrium is possible, and the density matrix will be of the form:

$$\rho = \frac{1}{\Xi} \exp [-\alpha\{\hbar\Delta S_z\} - \beta \mathcal{H}^0], \quad (2.2)$$

where Ξ is the normalization constant and α and β are proportional to the inverse spin temperatures of both systems, and have the dimension $1/kT$.

Under our experimental conditions ρ can be approximated by:

$$\rho = \frac{1}{\Xi} [1 - \alpha\{\hbar\Delta S_z\} - \beta \mathcal{H}^0]. \quad (2.3)$$

Now: $\Xi = \text{Tr}\{1\}$. From this density matrix the expectation value of the spin Hamiltonian in the rotating frame of reference can be calculated. The result is:

$$\begin{aligned} \langle \mathcal{H}'_{\text{spin}} \rangle &= \text{Tr}\{\rho \mathcal{H}'_{\text{spin}}\} = \\ &= \frac{1}{\text{Tr}\{1\}} [-\alpha \text{Tr}\{\hbar\Delta S_z\}^2 - \beta \text{Tr}\{\mathcal{H}^0\}^2] = \\ &= -\alpha[\frac{1}{4}N_e \hbar^2 A_z^2] - \beta[\frac{5}{16}N_e \hbar^2 A_z^2 + \frac{1}{4}N_p \hbar^2 \omega_p^2 + \frac{1}{4}N_e \hbar^2 \omega_L^2], \quad (2.4) \end{aligned}$$

where: N_e = the total number of Cu ions,

N_p = the total number of protons,

ω_L = defined by the equation: $\frac{1}{4}\beta N_e \hbar^2 \omega_L^2 = \text{Tr}\{\rho \mathcal{H}'_D\}$.

2.3. *The time dependence of α and β .* The spin systems described above are not in complete equilibrium owing to the microwave field and spin-lattice relaxation. So the density matrix, and thus the inverse spin temperatures α and β are still time dependent. The time dependence of the density matrix is given by the well known equation:

$$\frac{\partial \rho(t)}{\partial t} = -\frac{i}{\hbar} [\mathcal{H}, \rho(t)]. \quad (2.5)$$

Provotorov⁵ derived the master equation for the secular part $\rho_1(t)$ of $\rho(t)$. In his derivation the spin Hamiltonian in a rotating frame of reference has the general form:

$$\mathcal{G}'_{\text{spin}} = \hbar \Delta S_z + \frac{1}{2} \hbar \omega_1 \{S^+ + S^-\} + \mathcal{G}^0, \quad (2.6)$$

where \mathcal{G}^0 commutes with S_z and the second term is small compared to the other two.

The resulting master equation is:

$$\frac{d\rho_1(t)}{dt} = -\frac{1}{2} \pi \omega_1 P' [S^+(\mathcal{G}^0, -\Delta), [S^-(\mathcal{G}^0, +\Delta), \rho_1(t)]], \quad (2.7)$$

where the operators $S^\pm(\mathcal{G}^0, \mp \Delta)$ are obtained from S^\pm by first transforming to the interaction system, and then taking its Fourier transform:

$$S^\pm(\mathcal{G}^0, \mp \Delta) = \frac{1}{2\pi} \int_{-\infty}^{+\infty} dt e^{\pm i \Delta t} e^{(i/\hbar) \mathcal{G}^0 t} S^\pm e^{-(i/\hbar) \mathcal{G}^0 t}. \quad (2.8)$$

Furthermore, P' is an operator, which extracts the secular part from the operators on which it acts, and also eliminates singularities that might occur at certain values of Δ .

In the case of a density matrix of the form:

$$\rho_1(t) = \frac{1}{\mathcal{E}} \exp[-\alpha(t) \hbar \Delta S_z - \beta(t) \mathcal{G}^0], \quad (2.9)$$

eq.(2.7) yields equations for the time dependence of $\alpha(t)$ and $\beta(t)$. They are:

$$\frac{d\alpha(t)}{dt} = -\pi \omega_1^2 h(\Delta) [\alpha(t) - \beta(t)], \quad (2.10a)$$

$$\frac{d\beta(t)}{dt} = +\pi \omega_1^2 h(\Delta) \frac{\hbar^2 \Delta^2 \text{Tr}\{S_z^2\}}{\text{Tr}\{\mathcal{G}^0\}^2} [\alpha(t) - \beta(t)], \quad (2.10b)$$

where $h(\Delta)$ is a shape function of the form

$$h(\Delta) = \frac{\text{Tr}\{P'S^+(\mathcal{G}^0, -\Delta)S^-(\mathcal{G}^0, +\Delta)\}}{2\text{Tr}\{S_z\}^2} \quad (2.11)$$

These results can be used in the case of diluted Cu-Tutton salts without imposing any conditions beside those mentioned in the previous paragraph. Then $\mathcal{G}'_{\text{spin}}$ can be replaced by $\mathcal{H}'_{\text{spin}}$ and \mathcal{G}^0 by \mathcal{H}^0 and eqs. (2.10) and (2.11) can be used for the calculation of the time dependence of $\mathcal{H}'_{\text{spin}}$. However, before being able to solve $\alpha(t)$ and $\beta(t)$, we have to extend eqs. (2.10a) and (2.10b) with terms for spin-lattice relaxation. Furthermore we shall have to derive the shape function $h(\Delta)$ from eq. (2.11), and also calculate the magnitude of $\text{Tr}\{S_z\}^2/\text{Tr}\{\mathcal{H}^0\}^2$

Upon introducing eq. (2.1) for \mathcal{H}^0 in Cu-Tutton salt into eq. (2.11), $h(\Delta)$ can be derived to be of the form:

$$h(\Delta) = \frac{1}{4} \sum_{m=-\frac{3}{2}}^{m=+\frac{3}{2}} f(\Delta + mA_z); \quad (2.12)$$

$h(\Delta)$ is the shape of the total resonance spectrum of this salt. Each of the four terms $f(\Delta + mA_z)$ is the shape function of a single resonance line under the influence of the dipolar broadening \mathcal{H}'_D . These single resonance lines have their centres at $\Delta = -mA_z = \pm\frac{1}{2}A_z$ and $\pm\frac{3}{2}A_z$, where A_z is the hyperfine splitting constant introduced in eq. (2.1) (see fig. 2.1).

Secondly the magnitude of $\text{Tr}\{S_z\}^2/\text{Tr}\{\mathcal{H}^0\}^2$ was calculated in eq. (2.4) to be

$$\Delta^2 \left/ \left(\frac{5}{4}A_z^2 + \omega_L^2 + \frac{N_p}{N_e} \omega_p^2 \right) \right.$$

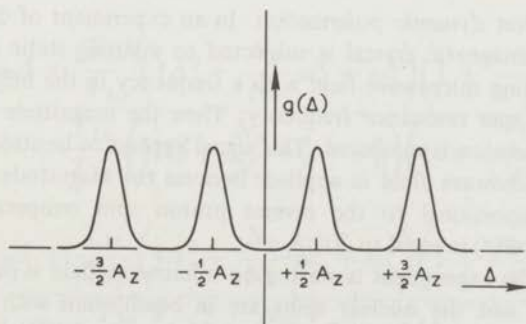


Fig. 2.1. The shape function $h(\Delta)$

The spin-lattice relaxation can be accounted for phenomenologically by adding two terms to eqs. (2.10a) and (2.10b). The electron Zeeman energy in the rotating frame, $\langle Z_e \rangle = -\alpha(t) [\frac{1}{4} N_e \hbar^2 \Delta^2]$, reaches its equilibrium value under influence of the lattice, $\langle Z_e \rangle_0 = -(\omega_e/\Delta) \beta_L [\frac{1}{4} N_e \hbar^2 \Delta^2]$ with a time constant T_{1e} . Here β_L is proportional to the inverse lattice temperature and has the dimension $1/kT$.

The proton Zeeman energy, $\langle Z_n \rangle = -\beta(t) [\frac{1}{4} N_p \hbar^2 \omega_p^2]$, reaches its equilibrium value with the lattice: $\langle Z_n \rangle_0 = -\beta_L [\frac{1}{4} N_p \hbar^2 \omega_p^2]$ with the nuclear relaxation time T_{1p} . So owing to spin-lattice relaxation only, $\alpha(t)$ and $\beta(t)$ will reach the equilibrium values $(\omega_e/\Delta) \beta_L$ and β_L with the time constants T_{1e} and T_{1p} respectively.

As a result of all these considerations the complete equations for the time dependence of $\alpha(t)$ and $\beta(t)$ will be:

$$\frac{d}{dt} \alpha(t) = -\pi \omega_1^2 \frac{1}{4} \sum_{m=-\frac{1}{2}}^{+\frac{1}{2}} f(\Delta + mA_z) [\alpha(t) - \beta(t)] +$$

$$-\frac{1}{T_{1e}} \left[\alpha(t) - \frac{\omega_e}{\Delta} \beta_L \right], \quad (2.13a)$$

$$\frac{d}{dt} \beta(t) = +\pi \omega_1^2 \frac{1}{4} \sum_{m=-\frac{1}{2}}^{+\frac{1}{2}} f(\Delta + mA_z) \frac{\Delta^2}{\frac{5}{4} A_z^2 + \omega_L^2 + \frac{N_p}{N_e} \omega_p^2} \times$$

$$\times [\alpha(t) - \beta(t)] - \frac{1}{T_{1p}} [\beta(t) - \beta_L]. \quad (2.13b)$$

From these equations the time behaviour of $\alpha(t)$ and $\beta(t)$ can be solved. Thus they enable us to calculate the time dependence of the proton and electron spin resonance signal in double resonance experiments.

2.4. Proton dynamic polarization. In an experiment of dynamic polarization a paramagnetic crystal is subjected to a strong static magnetic field, and a saturating microwave field with a frequency in the neighbourhood of the electron spin resonance frequency. Then the magnitude of the proton magnetic resonance is measured. This signal appears to be strongly enhanced, when the microwave field is applied. Because the magnitude of the N.M.R. signal is proportional to the inverse proton spin temperature $\beta(t)$, the enhancement $E(t)$ is equal to $\beta(t)/\beta_L$.

Before the experiment is started no microwave field is present and both the electron and the nuclear spins are in equilibrium with the lattice, so $\beta(t) = \beta_L$ or $E(t) = 1$ and the inverse temperature of the electron Zeeman system $\alpha(t) = (\omega_e/\Delta) \beta_L$. Then a microwave field with a frequency $\omega = \omega_e - \Delta$ is switched on, and both $\beta(t)$ and $\alpha(t)$ will change. Finally a new

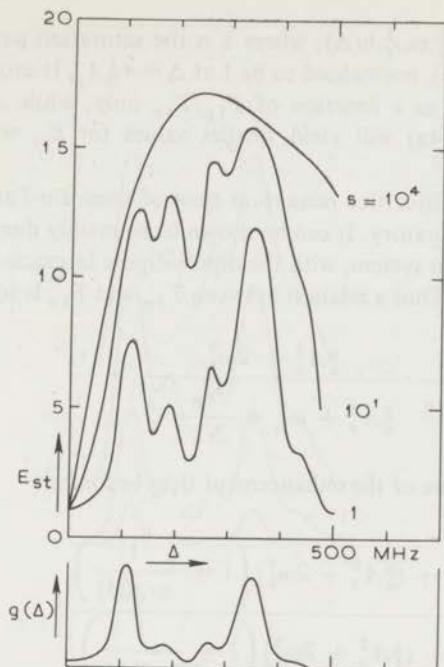


Fig. 2.2. E_{st} as a function of Δ for several values of s . The line shape was experimentally measured in $ZnK_2(SO_4)_2 \cdot 6H_2O$ containing 1% Cu. The static magnetic field was directed parallel to the b axis.

stationary state is reached, where $\alpha(t)$ and $\beta(t)$ have the stationary values α_{st} and β_{st} .

When an experiment of dynamic polarization is performed in Cu-Tutton salts eqs. (2.13a) and (2.13b) can be applied. From these we will first derive the stationary values, and later the time-dependent behaviour of $\beta(t)$.

The stationary solutions of eqs. (2.13a) and (2.13b) are:

$$E_{st} = \frac{\beta_{st}}{\beta_L} = \frac{\omega_e \Delta + \frac{T_{1e}}{T_{1p}} \left(\frac{5}{4} A_z^2 + \frac{N_p}{N_e} \omega_p^2 + \omega_L^2 \right) \left(1 + \frac{1}{s \cdot g(\Delta)} \right)}{\Delta^2 + \frac{T_{1e}}{T_{1p}} \left(\frac{5}{4} A_z^2 + \frac{N_p}{N_e} \omega_p^2 + \omega_L^2 \right) \left(1 + \frac{1}{s \cdot g(\Delta)} \right)}, \quad (2.14a)$$

$$\frac{\alpha_{st}}{\beta_1} = \frac{\omega_e \Delta + \frac{T_{1e}}{T_{1p}} \left(\frac{5}{4} A_z^2 + \frac{N_p}{N_e} \omega_p^2 + \omega_L^2 \right) \left(1 + \frac{\omega_e}{\Delta} \frac{1}{s \cdot g(\Delta)} \right)}{\Delta^2 + \frac{T_{1e}}{T_{1p}} \left(\frac{5}{4} A_z^2 + \frac{N_p}{N_e} \omega_p^2 + \omega_L^2 \right) \left(1 + \frac{1}{s \cdot g(\Delta)} \right)}. \quad (2.14b)$$

Here: $s \cdot g(\Delta) = T_{1e} \cdot \pi \omega_1^2 \cdot h(\Delta)$, where s is the saturation parameter and $g(\Delta)$ the line shape $h(\Delta)$, normalised to be 1 at $\Delta = +\frac{1}{2}A_z$. It should be noted that if E_{st} is regarded as a function of T_{1p}/T_{1e} only, while Δ and s are kept constant, eq. (2.14a) will yield smaller values for E_{st} when T_{1p}/T_{1e} decreases.

The proton spin-lattice relaxation time of these Cu-Tutton salts is being studied at our laboratory. It can be shown to be mainly due to the contact of the nuclear Zeeman system, with the dipole-dipole interaction system and the hyperfine system. Thus a relation between T_{1p} and T_{1e} is found to exist⁶:

$$\frac{1}{T_{1p}} \simeq \frac{1}{T_{1e}} \cdot \frac{\frac{5}{4}A_z^2 + 2\omega_L^2}{\frac{5}{4}A_z^2 + \omega_L^2 + \frac{N_p}{N_e} \omega_p^2}. \quad (2.15)$$

The stationary value of the enhancement then becomes:

$$E_{st} = \frac{\omega_e \Delta + (\frac{5}{4}A_z^2 + 2\omega_L^2) \left(1 + \frac{1}{s \cdot g(\Delta)}\right)}{\Delta^2 + (\frac{5}{4}A_z^2 + 2\omega_L^2) \left(1 + \frac{1}{s \cdot g(\Delta)}\right)}. \quad (2.16)$$

The time behaviour of $\beta(t)$ can be solved from eqs. (2.13a) and (2.13b). The solution of the two coupled equations is:

$$E(t) = \frac{\beta(t)}{\beta_L} = E_{st} - (E_{st} - E_2) e^{-t/\tau_1} - (E_2 - 1) e^{-t/\tau_2}, \quad (2.17)$$

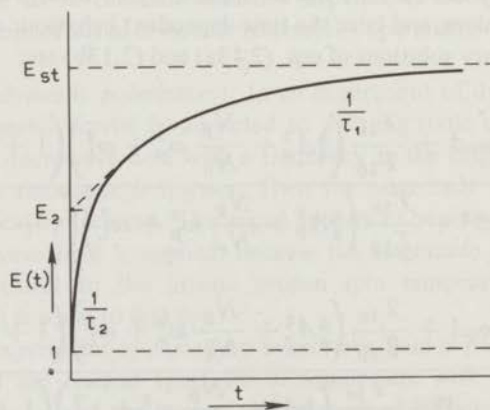


Fig. 2.3. The time behaviour of $E(t)$ according to eq. (2.17)

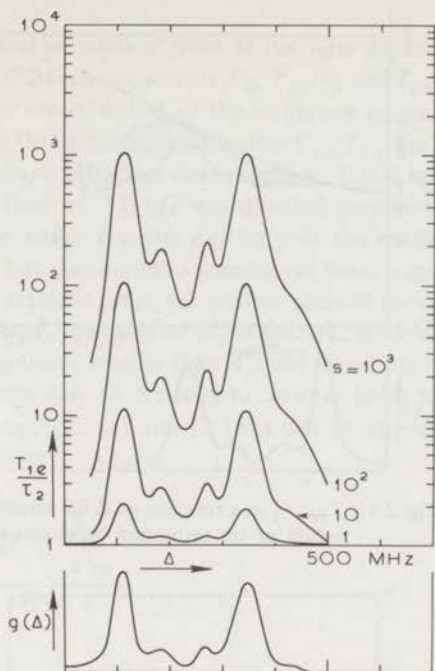


Fig. 2.4. T_{1e}/τ_2 as a function of Δ for several values of the saturation parameter s .

where:

$$\begin{aligned} \frac{T_{1e}}{\tau_{2,1}} = & \frac{1}{2} s \cdot g(\Delta) (B+1) \left[\left[1 + \frac{1}{s \cdot g(\Delta)} \cdot \frac{T_{1e}}{T_{1p}} + 1 \right] + \right. \\ & \pm \left[1 + \frac{2}{s \cdot g(\Delta)} \cdot \frac{(B-1) \left(\frac{T_{1e}}{T_{1p}} - 1 \right)}{(B+1)^2} + \right. \\ & \left. \left. + \left(\frac{1}{s \cdot g(\Delta)} \cdot \frac{T_{1e}}{B+1} - 1 \right)^2 \right]^{\frac{1}{2}} \right] \end{aligned} \quad (2.18a)$$

and:

$$E_2 = \frac{\frac{s \cdot g(\Delta)}{T_{1e}} \cdot B \cdot \left(\frac{\alpha_{st}}{\beta_L} - \frac{\omega_e}{\Delta} \right) + \left(\frac{1}{\tau_1} - \frac{s \cdot g(\Delta)}{T_{1e}} \cdot B - \frac{1}{T_{1p}} \right) \left(\frac{\beta_{st}}{\beta_L} - 1 \right)}{\frac{1}{\tau_1} - \frac{1}{\tau_2}} \quad (2.18b)$$

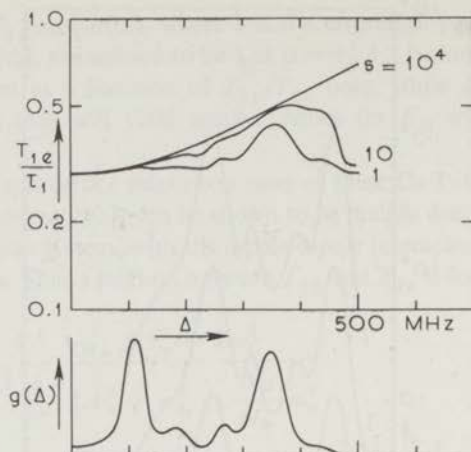


Fig. 2.5. T_{1e}/τ_1 as a function of Δ for several values of the saturation parameter s .

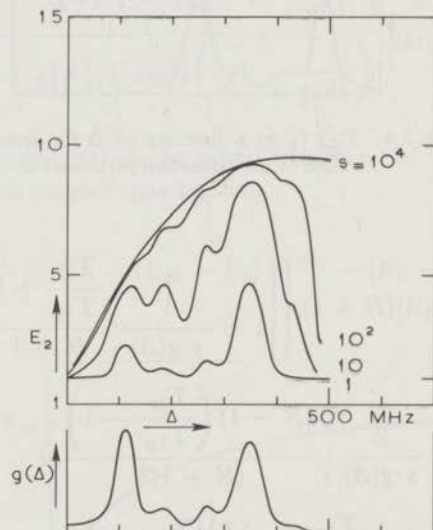


Fig. 2.6. E_2 as a function of Δ for several values of the saturation parameter s .

In these equations α_{st} , β_{st} and E_{st} are the stationary solutions obtained above in eqs. (2.14a) and (2.14b) while B is defined by:

$$B = \frac{\Delta^2}{\frac{5}{4}A_z^2 + \omega_L^2 + \frac{N_p}{N_e} \omega_p^2} \quad (2.19)$$

In fig. 2.3 a typical example is given of the time dependence of $E(t)$. In the figs. 2.4, 2.5 and 2.6 the quantities E_2 , T_{1e}/τ_2 and T_{1e}/τ_1 are plotted as a function of Δ for several values of the saturation parameter s , in the case of $\text{ZnK}_2(\text{SO}_4)_2 \cdot 6\text{H}_2\text{O}$ containing 1% Cu. For T_{1e}/T_{1p} the value of eq. (2.15) is used. The line shape $g(\Delta)$ was determined in E.S.R. experiments, where a static magnetic field of 3.0 kG was directed parallel to the b axis of the crystal. This line shape consists not only of the resonance lines discussed above (fig. 2.1), but also contains some small lines, originating in transitions, where beside the electron spins, the nuclear spins of the copper ions flip too¹. From this line shape, the value of A_z is derived, while ω_L^2 is estimated to be two orders of magnitude smaller than A_z^2 , and hence neglected.

In the extreme case of a strong microwave field, such that $s \gg 1$ (typically $s \approx 10^4$), eqs. (2.18a) and (2.18b) can be approximated by:

$$\frac{T_{1e}}{\tau_1} = \frac{B + \frac{T_{1e}}{T_{1p}}}{B + 1}, \quad (2.20a)$$

$$\frac{T_{1e}}{\tau_2} = s \cdot g(\Delta) \cdot (B + 1), \quad (2.20b)$$

$$E_2 = \frac{\frac{\omega_e}{\Delta} B + 1}{B + 1}. \quad (2.20c)$$

Under these circumstances the process of dynamic polarization can be described as proceeding in two successive steps. First an enhancement E_2 is reached with a time constant τ_2 , which is several orders of magnitude shorter than T_{1e} . This enhancement is the result of the large energy exchange between the electron Zeeman system and the combined nuclear Zeeman, hyperfine and dipole-dipole interaction system, effected by the microwave field. As eq. (2.20b) shows, the rate of this exchange, τ_2^{-1} , is proportional to the microwave power. In this first process spin-lattice relaxation can be neglected, so τ_2 contains the well measurable quantities N_e/N_p , ω_p , ω_e , Δ , and A_z only, and can thus be predicted accurately. When E_2 is reached, a much slower process appears, where the final enhancement E_{st} is reached with the time constant τ_1 . This latter process is mainly due to spin-lattice relaxation, so the magnitude of τ_1 will be of the order of T_{1e} . It can be seen from figs. 2.2 to 2.6 that E_2 is of the same order of magnitude as E_{st} , so all the quantities $1/\tau_1$, $1/\tau_2$, E_2 and E_{st} should be well measurable under the experimental conditions described above. In chapter IV measurements of

these quantities as a function of Δ and the microwave power will be given and compared with this theory.

3. *Theoretical description of distant ENDOR.* The theoretical description of distant ENDOR in diluted Cu-Tutton salts will be presented in two parts. First the equations for the time dependence of the inverse spin temperatures of the different spin systems, which are derived above (the eqs. 2.13a and 2.13b), will be extended to the case of distant ENDOR. In the second step their stationary and time dependent solutions are obtained, and with these solutions the behaviour of the microwave absorption signal owing to the distant ENDOR effect is determined.

3.1. *The equations for distant ENDOR.* In an experiment of distant ENDOR the E.S.R. signal is observed with a saturating microwave field. Then an rf field with a frequency ω_p saturating the proton spin resonance signal is applied. Owing to the distant ENDOR effect the E.S.R. signal changes and a new equilibrium magnitude of this signal is reached. The rate at which the microwave absorption signal changes and its total change can be calculated from the eqs. (2.13a) and (2.13b) if a term accounting for the rf field is added. This extra term can be derived as follows:

When an rf field with a frequency ω_p is applied, proton spin flips are induced with a rate W_N . According to Provotorov⁵ the energy absorbed per second from the rf field is then given by:

$$P_N = -W_N \left[\frac{1}{4} N_p h^2 \omega_p^2 \right] \beta$$

This energy flows into the extended nuclear spin system.* The total energy of this extended nuclear spin system was calculated in eq.(2.4) to be:

$$\langle \mathcal{H}^o \rangle = -\beta \left[\frac{5}{16} N_e \hbar^2 A_z^2 + \frac{1}{4} N_p \hbar^2 \omega_p^2 + \frac{1}{4} N_e \hbar^2 \omega_L^2 \right],$$

The conservation of energy requires that:

$$P_N = -\frac{\partial}{\partial t} \langle \mathcal{H}^o \rangle$$

Thus an equation for the time dependence of $\beta(t)$ owing to the rf field is obtained:

$$\left. \frac{\partial}{\partial t} \beta(t) \right)_{\text{rf field}} = -W_N \frac{\frac{N_p}{N_e} \omega_p^2}{\frac{N_p}{N_e} \omega_p^2 + \frac{5}{4} A_z^2 + \omega_L^2} \beta(t) = -\frac{s_N}{T_{1p}} \beta(t)$$

where the saturation parameter of the extended nuclear spin system s_N , is defined by:

* For brevity we denote the combined hyperfine, dipole-dipole interaction and nuclear Zeeman system as the extended nuclear spin system.

$$s_N = W_N T_{1p} \frac{\frac{N_p}{N_e} \omega_p^2}{\frac{N_p}{N_e} \omega_p^2 + \frac{5}{4} A_z^2 + \omega_L^2}$$

So finally the time dependence of the inverse spin temperatures in the case of the distant ENDOR is given by:

$$\frac{d}{dt} \alpha(t) = -\frac{s_E}{T_{1e}} [\alpha(t) - \beta(t)] + \frac{1}{T_{1e}} \left[\alpha(t) - \frac{\omega_e}{\Delta} \beta_L \right], \quad (2.21a)$$

$$\frac{d}{dt} \beta(t) = \frac{s_E}{T_{1e}} \cdot B [\alpha(t) - \beta(t)] - \frac{1}{T_{1p}} [\beta(t) - \beta_L] - \frac{s_N}{T_{1p}} \cdot \beta(t) \quad (2.21b)$$

where $s_E = s.g(\Delta)$ and B is given by eq. (2.19).

3.2 *The solutions of the equations for distant ENDOR.* In an experiment of distant ENDOR the E.S.R. absorption signal is measured with a saturating microwave field with a frequency ω . An equation for this microwave absorption signal was derived by Provotorov⁵ for a simple Hamiltonian consisting of an electron Zeeman term and a dipole-dipole interaction term:

$$p(\Delta, t) = -\frac{1}{4} N_e \hbar^2 \Delta \omega \frac{s_E}{T_{1e}} [\alpha(t) - \beta(t)] \quad (2.22)$$

It was pointed out in section 2.3 of this chapter, that the equations derived by Provotorov for the time dependence of α and β and also for $p(\Delta t)$ can also be used in the case of the spin Hamiltonian of a diluted Copper Tutton salt. Hence the E.S.R. signal in the case of diluted Copper Tutton salts is also given by eq. (2.22).

A typical example of an experiment of distant ENDOR in such a crystal is shown in fig. 2.7. In this figure the intensity of the microwave absorption signal is shown as a function of time. At $t = t_0$ the microwave field with a frequency $\omega \cong \omega_e$ is applied and α and β will reach the equilibrium values α_0 and β_0 which are the stationary solutions of the eqs. (2.13a) and (2.13b). A microwave absorption signal appears, which is proportional to $(\alpha_0 - \beta_0)$. At $t = t_1$ the rf field with a frequency $\omega = \omega_p$ is applied. As a result α and β and hence in general also the microwave absorption signal, which is proportional to $(\alpha - \beta)$, will change. According to eq. (2.22) the increment of this absorption signal is then given by:

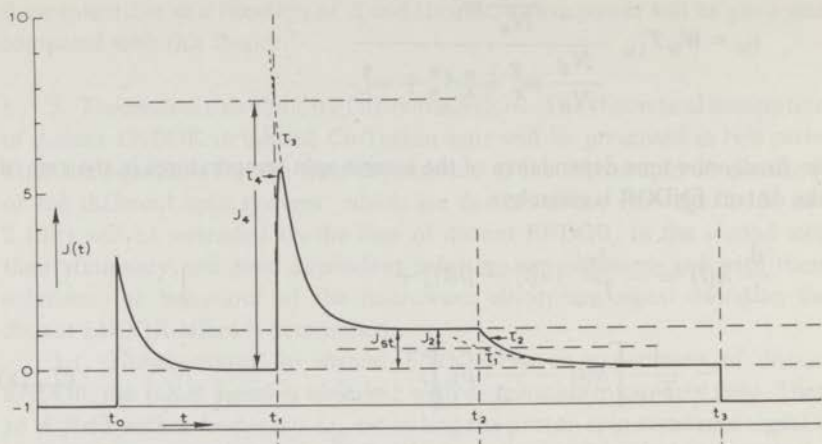


Fig. 2.7. A typical example of the time behaviour of $J(t)$ in an experiment of distant ENDOR.

$$J(t) = \frac{p(\Delta, t)}{p(\Delta, t_1)} - 1 = \frac{\alpha(t) - \beta(t)}{\alpha_0 - \beta_0} - 1 \quad (2.23)$$

Finally a new equilibrium state will be reached where α and β have equilibrium values α_{st} and β_{st} . The increment of the microwave absorption signal is then $J(t) = J_{st}$. The time dependence of $\alpha(t)$ and $\beta(t)$ and hence $J(t)$ after switching on the rf field can be solved from the eqs. (2.21a) and (2.21b).

At $t = t_2$ the rf field with a frequency ω_p is switched off again and α and β will return to their original values α_0 and β_0 . Hence the increment $J(t)$ will vanish. The time dependence of $J(t)$ after switching off the rf field can be solved from the eqs. (2.13a) and (2.13b).

In the next three sections we will deal theoretically with the stationary increment J_{st} , the time behaviour of $J(t)$ after switching on the rf field, and the time dependence of $J(t)$ after switching off the rf field.

3.3. *The stationary increment of the E.S.R. signal.* According to eq. (2.23) the stationary increment of the E.S.R. signal is defined by:

$$J_{st} = \frac{\alpha_{st} - \beta_{st}}{\alpha_0 - \beta_0} - 1 \quad (2.24)$$

where α_{st} and β_{st} are the stationary solutions of the eqs. (2.21a) and (2.21b) and α_0 and β_0 are the stationary solutions of the eqs. (2.13a) and (2.13b). These stationary solutions are:

$$\alpha_o = \frac{\frac{\omega_e}{\Delta} \cdot B + \frac{T_{1e}}{T_{1p}} \left[1 + \frac{\omega_e}{\Delta} \cdot \frac{1}{s_E} \right]}{B + \frac{T_{1e}}{T_{1p}} \left[1 + \frac{1}{s_E} \right]} \cdot \beta_L \quad (2.24a)$$

$$\beta_o = \frac{\frac{\omega_e}{\Delta} \cdot B + \frac{T_{1e}}{T_{1p}} \left[1 + \frac{1}{s_E} \right]}{B + \frac{T_{1e}}{T_{1p}} \left[1 + \frac{1}{s_E} \right]} \quad (2.24b)$$

$$\alpha_{st} = \frac{\frac{\omega_e}{\Delta} \cdot B + \frac{T_{1e}}{T_{1p}} \left[1 + \frac{\omega_e}{\Delta} \cdot \frac{1}{s_E} (1 + s_N) \right]}{B + \frac{T_{1e}}{T_{1p}} \left[1 + \frac{1}{s_E} \right] \cdot [1 + s_N]} \cdot \beta_L \quad (2.24c)$$

$$\beta_{st} = \frac{\frac{\omega_e}{\Delta} \cdot B + \frac{T_{1e}}{T_{1p}} \left[1 + \frac{1}{s_E} \right]}{B + \frac{T_{1e}}{T_{1p}} \left[1 + \frac{1}{s_E} \right] \cdot [1 + s_N]} \cdot \beta_L \quad (2.24d)$$

In fig. 2.8 calculated curves for J_{st} are plotted as a function of the electronic saturation parameter s_E , for several values of the saturation parameter of the extended nuclear spin system s_N , in the case of $ZnCs_2(SO_4)_2 \cdot 6H_2O$ containing 1% Cu. From E.S.R. experiments A_z was derived, while ω_L^2 was found to be two orders of magnitude smaller than A_z^2 and hence neglected. The static magnetic field is 3.0 kG, and Δ is chosen to be $+\frac{3}{2}A_z$. Eq. (2.15) is used to obtain the ratio T_{1e}/T_{1p} for the calculation of J_{st} in fig. 2.8.

Fig. 2.8 shows that J_{st} is strongly dependent on s_E for $s_E < 10^2$ and strongly dependent on s_N for $s_N < 10^2$. However, in the case of a strongly saturating microwave power (e.g. $s_E < 10^2$) and a strongly saturating rf field (e.g. $s_N > 10^2$), J_{st} is independent of s_E and s_N . Then J_{st} can be approximated by:

$$J_{st}^{max} = \frac{\frac{\omega_e}{\Delta} \cdot B + \frac{T_{1e}}{T_{1p}}}{\left(\frac{\omega_e}{\Delta} - 1\right) \frac{T_{1e}}{T_{1p}}} \quad (2.25)$$

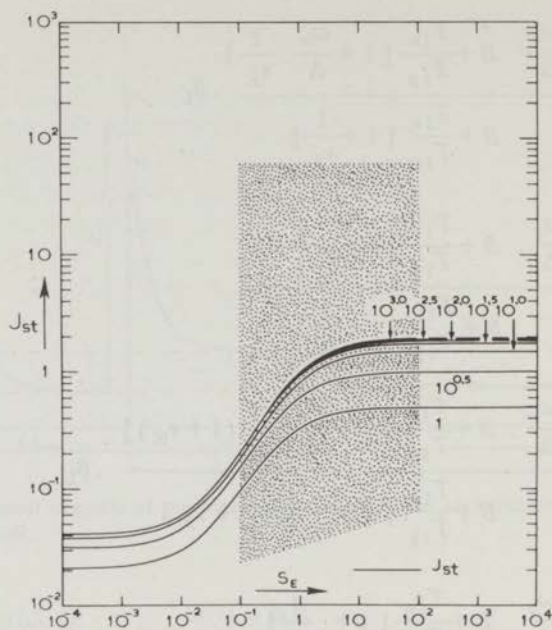


Fig. 2.8. Theoretical curves for J_{st} as a function of s_E for several values of s_N in the case of $ZnCs_2(SO_4)_2 \cdot 6H_2O$ containing 1% Cu.

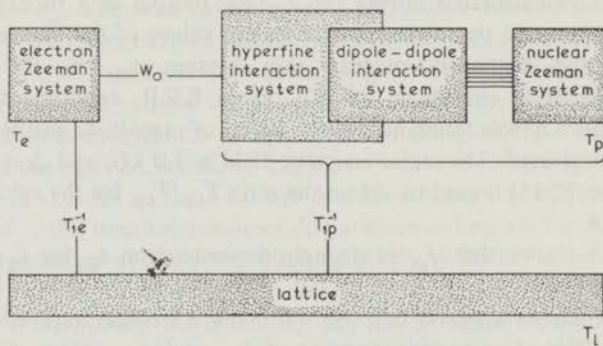


Fig. 2.9. Schematic representation of the spin systems in a dilute Copper Tutton salt.

Eq.(2.25) shows that J_{st}^{max} is strongly dependent on the ratio T_{1e}/T_{1p} . When the theoretical eq. (2.15) for this ratio is used, eq. (2.15) becomes simply:

$$J_{st} = \frac{\Delta^2}{\frac{5}{4}A_z^2 + 2\omega_L^2} \quad (2.26)$$

which is independent of N_p/N_e and thus of the concentration of the Cu^{2+} -ions in the sample.

The existence of the increment J_{st} , when the rf field is switched on, can also be accounted for in the following simple qualitative manner (see fig. 2.9). Owing to the rf field, which causes proton spin flips, a flow of energy exists from this rf field into the extended nuclear spin system. Part of this energy flows to the lattice. The microwave field creates a transport of the remaining part of the energy to the electron Zeeman system. The eqs. (2.21a) and (2.21b) show that this transport is only possible if the initial value of $(\alpha - \beta) : (\alpha_o - \beta_o)$ is increased to a larger value $\alpha_{st} - \beta_{st}$. Because, according to eq. (2.22) the microwave absorption signal is also proportional to $(\alpha - \beta)$, this increased value $\alpha_{st} - \beta_{st}$, which appears upon the application of the rf field, is observed as the distant ENDOR effect.

3.4. *The transient behaviour of $J(t)$ after switching on the rf field.* The time dependence of $J(t)$ after switching on the rf field to saturate the proton spin resonance signal can be solved from the eqs. (2.21a) and (2.21b). The solution of the two coupled equations is:

$$J(t) = J_{st} - (J_{st} - J_4)e^{-t/\tau_3} - J_4e^{-t/\tau_4} \quad (2.27)$$

In fig. 2.7 this behaviour is plotted, and the coefficients J_{st} and J_4 are shown. The time constants τ_3 and τ_4 are calculated to be:

$$\begin{aligned} \frac{T_{1e}}{\tau_{4,3}} &= \frac{1}{2} [s_E (B+1) + \frac{T_{1e}}{T_{1p}} (1+s_N) + 1] \pm \\ &\pm \frac{1}{2} [\{ s_E (B-1) + \frac{T_{1e}}{T_{1p}} (1+s_N) - 1 \}^2 + s_E^2 \cdot B]^{\frac{1}{2}} \end{aligned} \quad (2.28a)$$

while:

$$\begin{aligned} J_4 &= \frac{s_E (B+1) + \frac{T_{1e}}{T_{1p}} (1+s_N) - \frac{T_{1e}}{\tau_3}}{\frac{T_{1e}}{\tau_4} - \frac{T_{1e}}{\tau_3}} \cdot \frac{\beta_o - \beta_{st}}{\alpha_o - \beta_o} + \\ &\frac{s_E (B+1) + 1 - \frac{T_{1e}}{\tau_3}}{\frac{T_{1e}}{\tau_4} - \frac{T_{1e}}{\tau_3}} \cdot \frac{\alpha_o - \alpha_{st}}{\alpha_o - \beta_o} \end{aligned} \quad (2.28b)$$

In these equations α_o , β_o , α_{st} and β_{st} are the stationary solutions obtained

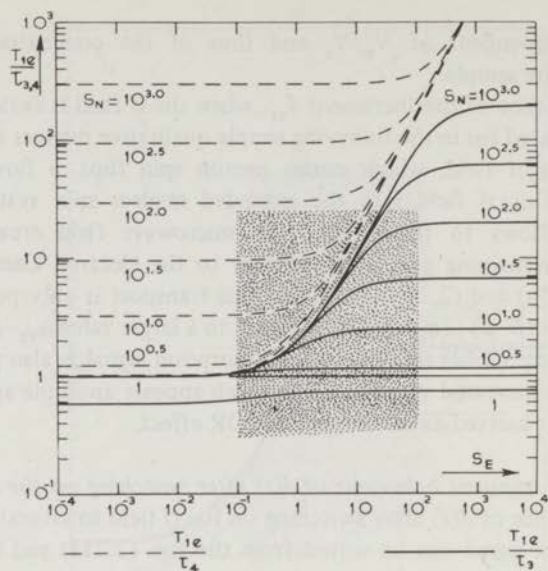


Fig. 2.10. Theoretical curves for T_{1e}/τ_3 and T_{1e}/τ_4 as a function of s_E for several values of s_N in the case of $ZnCs_2(SO_4)_2 \cdot 6H_2O$ containing 1% Cu.

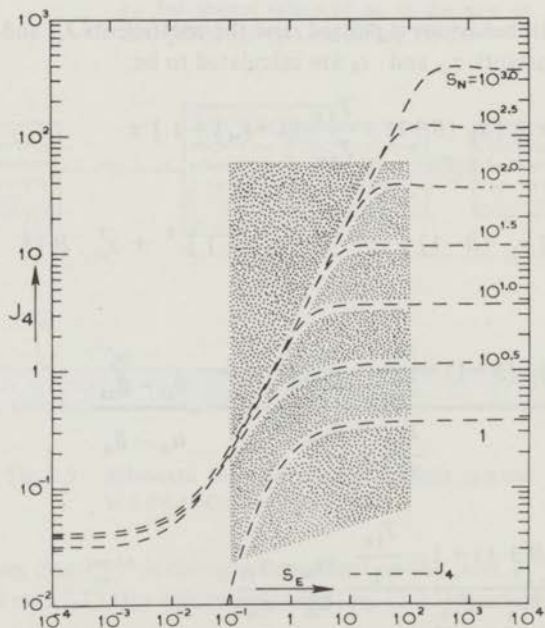


Fig. 2.11. Theoretical curves for J_4 as a function of s_E for several values of s_N in the case of $ZnCs_2(SO_4)_2 \cdot 6H_2O$ containing 1% Cu.

above in formulae (2.24a) to (2.24d). In fig. 2.10, T_{1e}/τ_3 and T_{1e}/τ_4 are plotted as a function of s_E for several values of s , again for $\text{ZnCs}_2(\text{SO}_4)_2 \cdot 6\text{H}_2\text{O}$ containing 1% Cu. For T_{1e}/T_{1p} the value of eq. (2.15) is used. The values used for A_z , ω_L , ω_e , ω_p and Δ are the same as for fig. 2.8. In fig. 2.11, J_4 is plotted as a function of s_E for several values of s_N in the same case as T_{1e}/τ_3 and T_{1e}/τ_4 in fig. 2.10 using the same values for B and T_{1e}/T_{1p} .

In the extreme case of a very strong microwave field so that the saturation parameter of the E.S.R. signal $s_E \gg 1$, and a very strong rf field so that the saturation parameter of the proton spin resonance signal $s_N \gg 1$, the eqs. (2.28a) and (2.28b) for τ_4 , τ_3 and J_4 can be greatly simplified. Two cases are to be distinguished: In the first case the rate at which the rf field induces proton spin flips is much larger than the rate at which the microwave field induces electron spin flips ($W_N \gg W_o$). In the second case $W_o \gg W_N$.

In the first case, when s_E , $s_N \gg 1$ and $W_N \gg W_o$, the eqs. (2.28a) and (2.28b) can be approximated by:

$$\frac{T_{1e}}{\tau_3} = s_E \cdot \frac{T_{1e}}{T_{1p}} \quad (2.29a)$$

$$\frac{T_{1e}}{\tau_4} = s_N \quad (2.29b)$$

$$J_4 = J_{st} \cdot s_E = \frac{\frac{\omega_e}{\Delta} \cdot B + \frac{T_{1e}}{T_{1p}}}{\left(\frac{\omega_e}{\Delta} - 1\right) \frac{T_{1e}}{T_{1p}}} \cdot s_E \quad (2.29c)$$

As can be seen from the figs. 2.10 and 2.11 the approximations given in the eqs. (2.29a), (2.29b) and (2.29c) typically hold when $s_E = 10$ and $s_N = 10^3$.

The main features of the eqs. (2.27), (2.29a), (2.29b) and (2.29c), describing the transient behaviour of $J(t)$ after switching on the rf field, can also be deduced with the help of the figs. 2.7 and 2.9 in the following simple qualitative manner. This transient behaviour can then be described as proceeding in two steps. First the rf field strongly saturates the extended nuclear spin system. The rate of this process, τ_4^{-1} , is mainly determined by the term $(s_N/T_{1p})\beta$ in eq. (2.21b) and τ_4^{-1} is proportional to s_N . Owing to the vanishing of β the E.S.R. signal, which according to eq. (2.22) is proportional to $(\alpha - \beta)$, will increase. The increment is then finally given by $J_4 = \frac{\alpha_o}{\alpha_o - \beta_o} - 1$

When J_4 is reached, a much slower process occurs by which the electron Zeeman system, the extended nuclear spin system and the lattice reach a final equilibrium with each other. Because $s_E \gg 1$, in this process the transitions

owing to the microwave field are much more influential than the transitions owing to the spin-lattice relaxation. So the rate of this second process, τ_3^{-1} , will be proportional to s_E .

In the second case, when $s_E, s_N \gg 1$ and $W_o \gg W_N$, the eqs. (2.28a) and (2.28b) can be approximated by:

$$\frac{T_{1e}}{\tau_3} = s_N \cdot \frac{T_{1e}}{T_{1p}} \cdot \frac{1}{B+1} \quad (2.30a)$$

$$\frac{T_{1e}}{\tau_4} = s_E \cdot (B+1) \quad (2.30b)$$

$$J_4 = J_{st} \cdot s_N \cdot \frac{T_{1e}}{T_{1p}} \cdot \frac{1}{B+1} \quad (2.30c)$$

As can be seen from the figs. 2.10 and 2.11 these approximations typically hold when $s_E = 10^3$ and $10 \leq s_N \leq 10^3$. As in the case of $s_E, s_N \gg 1$ and $W_o \ll W_N$, the main features of the eqs. (2.27), (2.30a), (2.30b) and (2.30c), describing the behaviour of $J(t)$ after switching on the rf field, can be deduced in a simple manner: (see the figs. 2.7 and 2.9). In this case ($s_E, s_N \gg 1, W_o \gg W_N$) the microwave field establishes a thermal equilibrium between the electron Zeeman system and the extended nuclear spin system. According to the eqs. (2.21a) and (2.21b) this thermal equilibrium is maintained by a flow of energy between these two spin systems proportional to s_E and $(\alpha - \beta)$. When the rf field inducing proton spin flips is switched on, a flow of rf energy into the extended nuclear spin system is created, and the equilibrium between the extended nuclear spin system and the electron Zeeman system is disturbed. Then two processes take place successively: In the first process a new thermal equilibrium between the extended nuclear spin system and the electron Zeeman system is reached under influence of the microwave field. The rate of this process τ_4^{-1} is proportional to the power of this microwave field and hence to s_E . Then a second and much slower process occurs, during which both systems are heated by the rf field until α and β reach their final equilibrium values α_{st} and β_{st} with this rf field and the lattice. Because $s_N \gg 1$, in this second process the transitions of the proton spins owing to the rf power dominate compared to spin-lattice relaxation processes, and the rate of this second process, τ_3^{-1} , will be proportional to s_N .

3.5. *The transient behaviour of $J(t)$ after switching off the rf field.* The time behaviour of $J(t)$ after switching off the rf field saturating the proton spin resonance signal, can be solved from the eqs. (2.13a) and (2.13b). The solution of the two coupled equations is:

$$J(t) = (J_{st} - J_2)e^{-t/\tau_1} + J_2e^{-t/\tau_2} \quad (2.31)$$

In fig. 2.7 this behaviour is plotted and the coefficients J_{st} and J_2 are shown. The time constants τ_1 and τ_2 are given by:

$$\begin{aligned} \frac{T_{1e}}{\tau_{2,1}} = & \frac{1}{2} s_E \cdot (B + 1) \left[\left[1 + \frac{1}{s_E} \cdot \frac{T_{1e} + 1}{B + 1} \right] + \right. \\ & \pm \left[1 + \frac{2}{s_E} \cdot \frac{(B - 1) \left(\frac{T_{1e}}{T_{1p}} - 1 \right)}{(B + 1)^2} + \right. \\ & \left. \left. + \left(\frac{1}{s_E} \cdot \frac{T_{1e} - 1}{B + 1} \right)^2 \right] \right] \quad (2.32) \end{aligned}$$

The eqs. (2.13a) and (2.13b) used to obtain these results are exactly the same as those used in the case of proton dynamic polarization. Hence the time constants τ_1 and τ_2 found in this experiment of distant ENDOR must be exactly the same as those found in an experiment of dynamic polarization. In chapter V measurements of τ_1 and τ_2 as a function of s_E by means of distant ENDOR, as well as dynamic polarization, will be presented and compared with each other and with the theory.

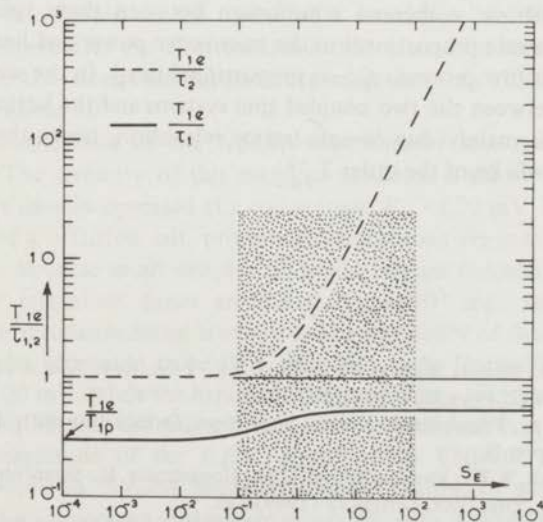


Fig. 2.12. Theoretical curves for T_{1e}/τ_1 and T_{1e}/τ_2 as a function of s_E in the case of $\text{ZnCs}_2(\text{SO}_4)_2 \cdot 6\text{H}_2\text{O}$ containing 1% Cu.

In fig. 2.12 the theoretical values of T_{1e}/τ_1 and T_{1e}/τ_2 are plotted as a function of s_E in the case of $\text{ZnCs}_2(\text{SO}_4)_2 \cdot 6\text{H}_2\text{O}$ containing 1% Cu^{2+} ions. For T_{1e}/T_{1p} the theoretical eq. (2.15) is used. For B the same value as in the figs. 2.8, 2.10 and 2.11 is used.

In the extreme case of a strong microwave field so that $s_E \gg 1$, eq. (2.32) can be approximated by:

$$\frac{T_{1e}}{\tau_1} = \frac{B + \frac{T_{1e}}{T_{1p}}}{B + 1},$$

$$\frac{T_{1e}}{\tau_2} = s_E \cdot (B + 1),$$

As can be seen from fig. 2.12 these approximations typically hold when $s_E \gg 10$.

The main features of the eqs. (2.31), (2.33a) and (2.33b) describing the transient behaviour of $J(t)$ after switching off the rf field can also be deduced in the following simple qualitative manner (see fig. 2.9). This transient behaviour can then be described as proceeding in two steps (see fig. 2.7). Before the rf field is turned off, a steady flow of energy from the rf field into the nuclear spin system and from that system into the electron Zeeman system exists. When the rf field is turned off this flow of energy ceases, and a new equilibrium between these two spin systems is established. As has been pointed out above a thermal equilibrium between these spin systems is reached with a rate proportional to the microwave power and hence to s_E . So the rate of this first process, τ_2^{-1} , is proportional to s_E . In the second step the equilibrium between the two coupled spin systems and the lattice is restored. This process is mainly due to spin-lattice relaxation, hence the rate of this process, τ_1^{-1} , will be of the order T_{1e}^{-1} .

REFERENCES

1. Bleaney, B., Bowers, K.D. and Ingram, D.J.E., Proc. Roy. Soc. A 228 (1955) 147.
2. Redfield, A.G., Phys. Rev. 98 (1955) 1787.
3. Abragam, A., Principles of Nuclear Magnetism, Oxford University Press (London, 1961, Chapter II.
4. Wenckebach, W.Th., Van den Heuvel, G.M., Hoogstraate, H., Swanenburg, T.J.B. and Poulis, N.J., Phys. Rev. Letters 22 (1969) 581.
5. Provotorov, B.N., Zh. eksper. teor. Fiz. 41 (1961) 1582, Soviet Physics JETP. 14 (1962) 1126.
6. Van den Heuvel, G.M., and Poulis, N.J., Physica, to be published.

CHAPTER III

THE EXPERIMENTAL ARRANGEMENT

The Arrangement, Elia Kazan (1970)

The experiments of nuclear dynamic polarization were performed with an X-band microwave apparatus to induce E.S.R. transitions and an N.M.R. spectrometer in the frequency range from 10 to 14 MHz. A block diagram of the apparatus is shown in fig. 3.1. The construction of the cavity is shown in fig. 3.2. The microwave power is supplied by a Varian V-58 C klystron. A calibrated attenuator of 0 - 60 dB is used to vary this microwave power. The klystron output power is measured by a bolometer, while a second bolometer is used to measure the power reflected by the cavity. Thus the microwave power dissipated in the cavity, P_E , can be determined. P_E can be varied by the calibrated attenuator from 0.2 W to 0.2 μ W. Then in the case of a Zn Tutton salt containing 1% Cu^{2+} -ions, transition probabilities varying from $6 \cdot 10^{-2} \text{ sec}^{-1}$ to $6 \cdot 10^4 \text{ sec}^{-1}$ can be obtained, when the microwave frequency is adjusted to the centre of a resonance line. Because at liquid Helium temperatures the electron spin-lattice relaxation time is of the order of 10 sec., the electronic saturation parameter s can thus be varied from about 1 to about 10^6 .

The central unit of the N.M.R. spectrometer is a modified Colpitts oscillator. The circuitry of this marginal oscillator is shown in fig. 3.3. This oscillator is usually operated at a coil voltage, V_c , of 20 mV. Then in the case of a diluted Cu-Tutton salt, proton spin transitions are induced at a rate of 10^{-5} sec^{-1} . Because in all samples, at liquid Helium temperatures the proton spin-lattice relaxation times are shorter than 10^3 sec ., saturation of the proton spin resonance signal is avoided. The sensitivity of the N.M.R. spectrometer can be estimated to be 10^{19} spins per gauss linewidth, at 1 K, a coil voltage of 20 mV, while the bandwidth of the receiver is chosen to be 1 Hz. It should be noted, that the filling factor of the N.M.R. coil is only about 5%.

The magnitude of the E.S.R. signal in the ENDOR experiments determined with an X-band superheterodyne microwave spectrometer. The proton spin resonance transitions are saturated with a Rohde and Schwartz power signal generator type SMLR.BN 41001. The construction of the cavity is the same as in the case of the nuclear dynamic polarization experiments. A

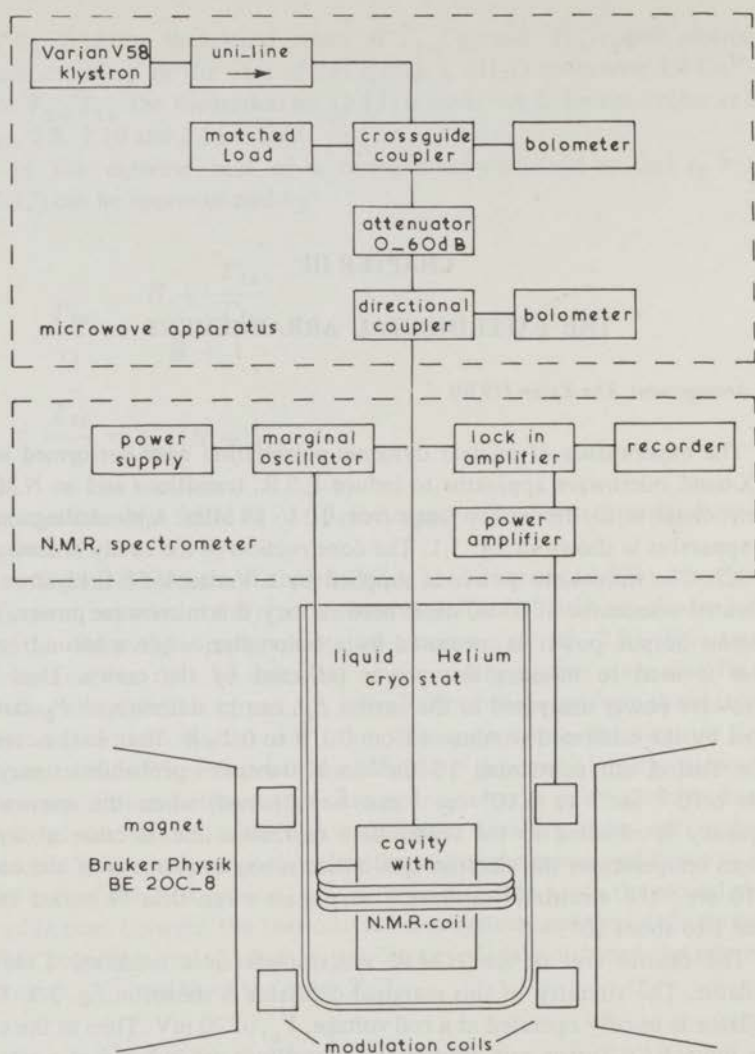


Fig. 3.1. Block diagram of the experimental arrangement for experiments of nuclear dynamic polarization.

block diagram of the complete ENDOR equipment is given in fig. 3.4. The monitor of the microwave spectrometer is a Varian VA 201 B klystron, which has a maximum output power of about 70 mW. As can be seen from fig. 3.4. this microwave power is fed into the cavity via a calibrated attenuator of 0-120 dB and a directional coupler. This directional coupler attenuates the microwave power with 10 dB, so the maximum power that can be fed into the cavity is about 7 mW. The procedure to measure the power reflected by the cavity is as follows. First it is mixed with the output of a local oscillator,

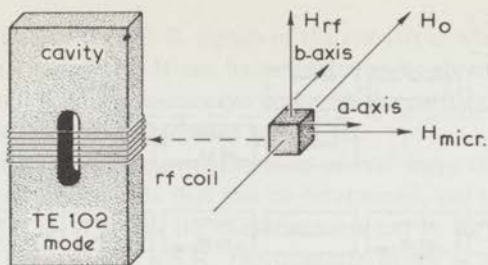


Fig. 3.2. The construction of the cavity and the orientation of the sample in the cavity in the case of the experiments of nuclear dynamic polarization as well as distant ENDOR.

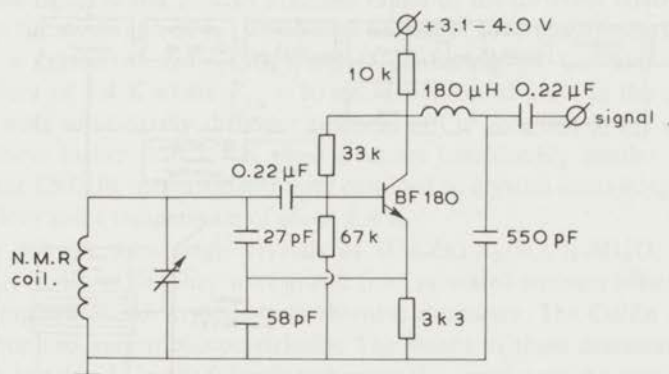


Fig. 3.3. Circuitry of the modified Colpitts oscillator.

which is tuned to a frequency 30 MHz higher than the frequency of the monitor. Then it is amplified by a 30 MHz L.E.L. amplifier and detected. The resulting DC voltage V_m is measured with a Philips PR 2500/00 recorder. A change of the microwave absorption in the cavity owing to E.S.R. will result in a change of the microwave power reflected by this cavity, and hence a change of the measured DC voltage V_m . It can be proved that when the monitor klystron is tuned to the exact resonance frequency of the cavity, the change of V_m is in first order proportional to the microwave power absorbed owing to the E.S.R.

The experimental arrangement contains two devices to stabilize the output frequencies of the two klystrons. In the first place the output frequency of the monitor is maintained at the resonance frequency of the cavity by frequency-modulating the output of this klystron with a 10 kHz signal. When the monitor is tuned to the exact resonance frequency of the cavity no 10 kHz modulation of the measured DC voltage V_m will be found.

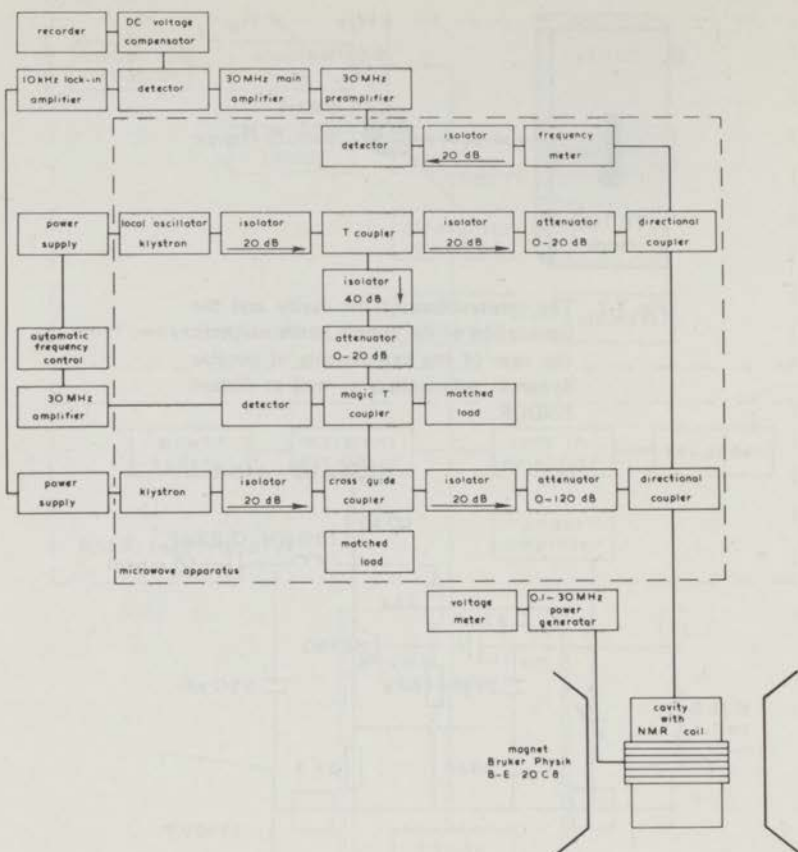


Fig. 3.4. Block diagram of the experimental arrangement for experiments of distant ENDOR.

However, when the monitor is tuned to a frequency slightly above or below the resonance frequency of the cavity, a 10 kHz modulation of V_m appears. As can be seen from fig. 3.4 this 10 kHz signal is fed into a 10 kHz lock-in amplifier. The output voltage of this 10 kHz lock-in amplifier is added to the reflector voltage of the monitor and thus the frequency of this klystron is corrected.

The frequency of the local oscillator is maintained at a value of 30 MHz above the frequency of the monitor by mixing a sample of the output of the monitor with a sample of the output of the local oscillator. The resulting signal is amplified with a 30 MHz amplifier and detected on a 30 MHz discriminator circuit. The resulting DC voltage is added to the reflector voltage of the local oscillator and thus the frequency of this klystron is corrected.

The sensitivity of the microwave spectrometer was estimated from the

signal to noise ratio of the E.S.R. signals of the crystals in which the ENDOR experiments were performed. It can be estimated to be about 10^{14} spins per gauss linewidth at 1 K and a microwave power in the cavity of 10 nW, while the bandwidth of the receiver is chosen to be 1 Hz.

Our experimental arrangement limits in several ways the values of the time-constants and coefficients that can be determined, and the values of the parameters s_E and s_N at which the measurements can be carried out. Owing to the response time of the E.S.R. spectrometer which is about 0.15 sec., only time constants larger than 0.3 sec. can be measured. s_N is limited by the maximum rf power (at a coil voltage of 9 V) on the N.M.R. coil that can be applied without heating the crystal. Finally s_E is limited at high microwave power by instabilities of the E.S.R. spectrometer and at low microwave power by the signal to noise ratio of the increment.

In the figs. 2.8 and 2.10 to 2.12 the values of the different coefficients and time constants and of s_E , which were accessible for measurements in the case of a crystal of $ZnCs_2(SO_4)_2 \cdot 6H_2O$ containing 1% Cu^{2+} ions and a temperature of 1.4 K where $T_{1e} = 30$ sec., are coloured gray. In the case of crystals with substantially different amounts of Cu^{2+} ions and in the case of temperatures higher than 1.4 K these areas are considerably smaller. Hence the distant ENDOR measurements were confined to crystals containing about 1% Cu^{2+} ions and a temperature of about 1.4 K.

The samples were single crystals of $(Cu,Zn) X_2(SO_4)_2 \cdot 6H_2O$, where $X = NH_4, K, Rb$ or Cs . They were grown from saturated aqueous solutions at room temperature. All crystals have rhombic symmetry. The Cu/Zn ratio c was determined spectrophotometrically. The results of these determinations are given in table 1. In the following chapters the samples will be denoted by

Table 1 The spectrophotometrically determined concentrations of the samples.

$c' \backslash X$	NH_4	K	Rb	Cs
2 %		2.09%		
1 %	0.90%	0.93%	0.48%	1 %
0.5%		0.50%		
0.2%		0.20%		
0.1%		0.11%		

the Cu/Zn ratio c' in the solutions from which the crystals were grown and by the monovalent ion in the crystals. So e.g. the sample of $ZnK_2(SO_4)_2 \cdot 6H_2O$ where $c = 2.09\%$ will be denoted by 2% CuKS.

CHAPTER IV

THE EXPERIMENTS OF NUCLEAR DYNAMIC POLARIZATION

Blow Up, Michelangelo Antonioni (1967)

In chapter II the theory was given of the dynamic polarization of the protons in Cu-Tutton salts. Formulae for the stationary and the transient behaviour of the enhancement of the proton magnetic resonance signal were obtained. In order to verify the theoretical results, experiments of proton dynamic polarization were performed in all crystals of table 1. (chapter III) The results of the measurements will be presented in two parts. First the stationary behaviour of the dynamic polarization will be discussed, secondly the transient behaviour. In both cases the experimental results will be compared with the theoretical formulae of chapter II.

1. *The stationary behaviour of the dynamic polarization.* When the microwave power is switched on the proton spin resonance signal reaches an equilibrium magnitude, which is enhanced by a factor E_{st} , compared to its thermal equilibrium value. This enhancement, E_{st} , was measured as a function of the microwave frequency ω and the microwave power P_E in all crystals mentioned above.

1.1. *CuKS.* The measured values of the stationary enhancement in the 0.5% CuKS sample are given on the right hand side of fig. 4.1. They were carried out at a static magnetic field of about 3.0 kG and at a temperature of 4.2 K. In this figure E_{st} is plotted for several values of P_E as a function of $\Delta = \omega_e - \omega$. ω_e is the Larmor frequency of the electron spin S of the Cu-ion in the static magnetic field H_0 . All these experiments were repeated at a lower temperature. The results of these measurements are essentially the same as in the case of 4.2 K. As an example the results for $P_E = 2$ mW and $T = 1.5$ K are represented by a dotted line in fig. 4.1.

In order to compare these experimental results with the theory given in chapter II, theoretical curves for E_{st} as a function of Δ are plotted on the left hand side of fig. 4.1 for several values of the saturation parameter s . This saturation parameter was defined in chapter II by the equation:

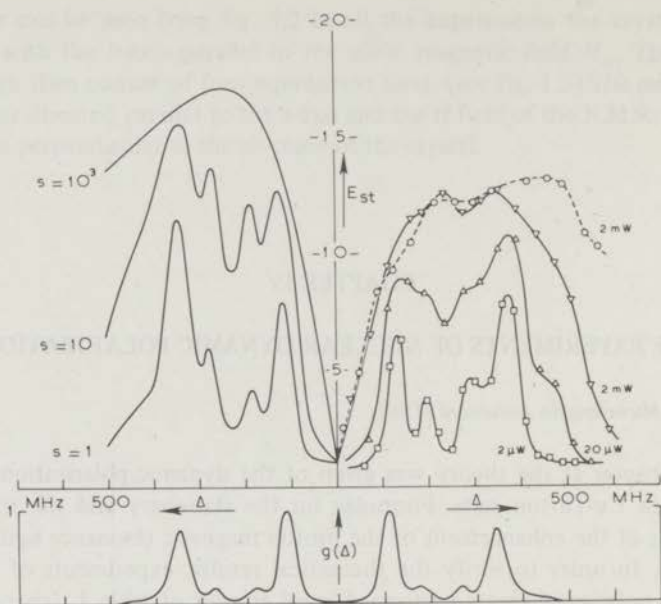


Fig. 4.1. The stationary enhancement E_{st} as a function of Δ for several values of P_E in 0.5% CuKS. The experimental curves were obtained at about 3.0 kG, while T was 4.2 K and 1.5 K.

$$W(\Delta) = s \cdot g(\Delta) / T_{1e}$$

where $W(\Delta)$ is the transition probability induced by the microwave field, $g(\Delta)$ is the shape function of the E.S.R. spectrum normalised to be 1 at $\Delta = \frac{1}{2}A_z$, and T_{1e} is the electron spin-lattice relaxation time. According to this definition s is proportional to W and hence to the microwave power P_E . The theoretical curves in fig. 4.1 are obtained by using formula 2.14a of chapter II:

$$E_{st} = \frac{\omega_e \Delta + \frac{T_{1e}}{T_{1p}} \left(\frac{5}{4} A_z^2 + \frac{N_p}{N_e} \omega_p^2 + \omega_L^2 \right) \left(1 + \frac{1}{s \cdot g(\Delta)} \right)}{\Delta^2 + \frac{T_{1e}}{T_{1p}} \left(\frac{5}{4} A_z^2 + \frac{N_p}{N_e} \omega_p^2 + \omega_L^2 \right) \left(1 + \frac{1}{s \cdot g(\Delta)} \right)} \quad (4.1)$$

Here A_z originates in the term $\hbar A_z S_z I_z'$ of the hyperfine interaction of the electron spins and the nuclear spin I' of the copper ion. Furthermore $\hbar \omega_L / \gamma_e$ is the local field caused by all other spin-spin interactions and ω_p is the Larmor frequency of the proton spins. Finally N_p is the total number of

proton spins and N_e the total number of electron spins in the crystal. For the calculation of the theoretical curves in fig. 4.1 the shape function $g(\Delta)$ and the parameters A_z and ω_L were determined from an E.S.R. experiment in the crystal.

The value of eq. (2.15) for the ratio T_{1e}/T_{1p} of the spin-lattice relaxation times of the electron spins and of the nuclear spins was inserted into eq. (4.1) to obtain the theoretical curves in figure 4.1.

We shall compare the theoretical and experimental curves in fig. 4.1 on two major features: the dependence of E_{st} on Δ and the maximum enhancement that has been obtained. For weak microwave power, E_{st} as a function of Δ exhibits a pronounced structure which closely resembles the line shape function $g(\Delta)$ of the E.S.R. spectrum. This structure disappears in the limit of high microwave power. From the theoretical curves in fig. 4.1 one can see that this structure can be completely accounted for by the theoretical predictions of formula 4.1. Furthermore the disappearance of this structure at high microwave power was also predicted theoretically.

The maximum enhancement that has been obtained experimentally, E_{st}^{max} , was 12.7 at 4.2 K and 13.2 at 1.5 K. The measuring accuracy of these values was about 10% owing to the low signal to noise ratio of the unenhanced proton signal. Hence E_{st}^{max} may be considered to be temperature independent as was predicted by eq. (4.1) and by the temperature independence of the ratio T_{1e}/T_{1p} in eq. (2.15).

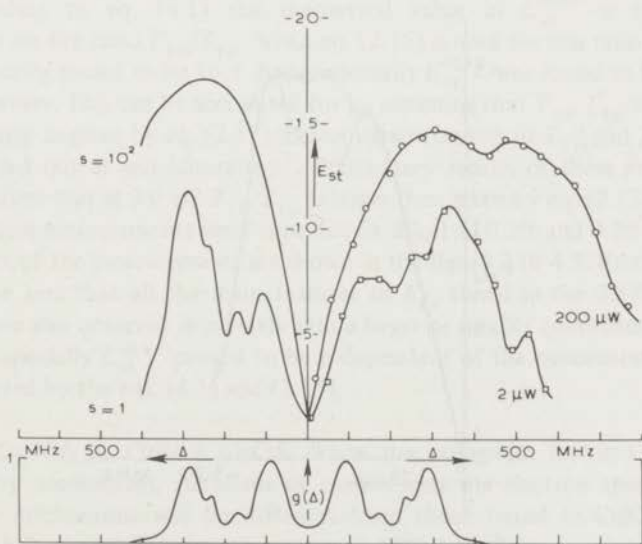


Fig. 4.2. The stationary enhancement E_{st} as a function of Δ for several values of P_E in 2% CuKS. The experimental curves were obtained at about 3.0 kG, while T was 4.2 K.

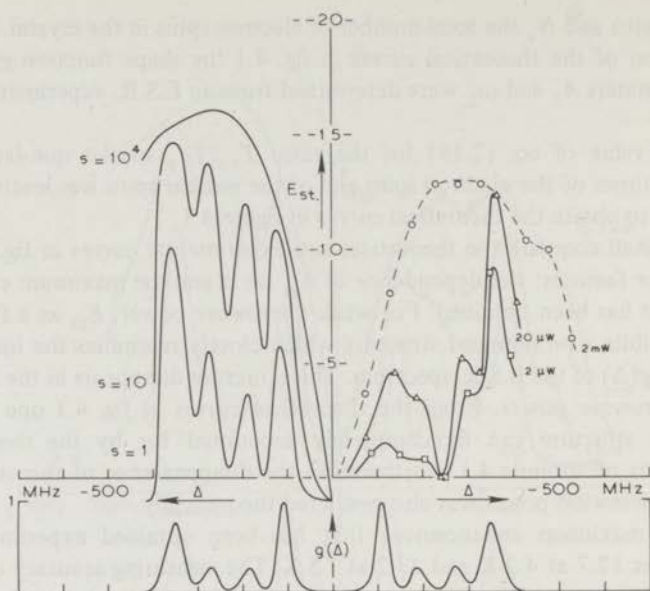


Fig. 4.4. The stationary enhancement E_{st} as a function of Δ for several values of P_E in 0.2% CuKS. The experimental curves were obtained at about 3.0 kG while T was 4.2 K and 2.0 K.

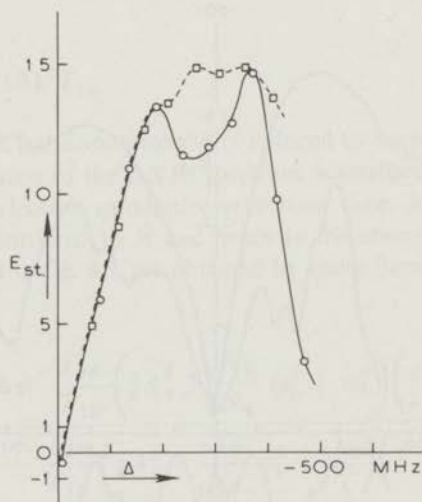


Fig. 4.5. The stationary enhancement E_{st} as a function of Δ for $P_E = 2$ mW in 0.1% CuKS. The experimental curves were obtained at about 3.0 kG while T was 4.2 K and 2.0 K.

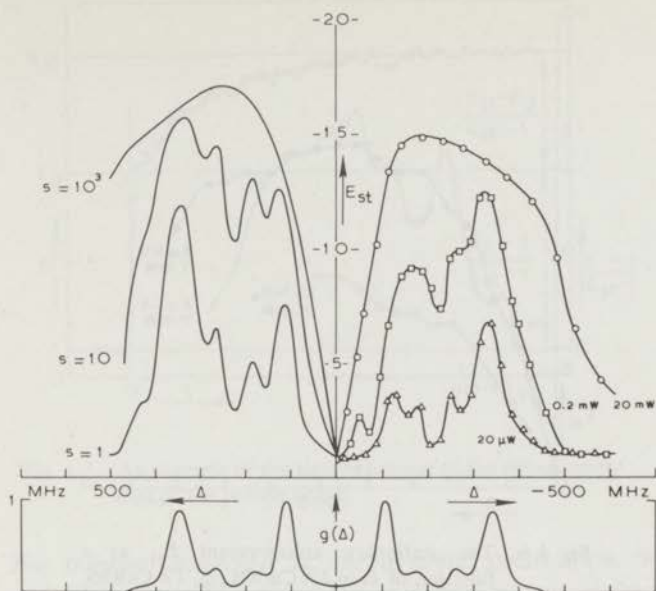


Fig. 4.3. The stationary enhancement E_{st} as a function of Δ for several values of P_E in 1% CuKS. The experimental curves were obtained at about 3.0 kG, while T was 4.2 K.

According to eq. (4.1) the theoretical value of E_{st}^{max} is strongly dependent on the ratio T_{1e}/T_{1p} . When eq. (2.15) is used for this ratio, E_{st}^{max} is theoretically found to be 16.5. Experimentally E_{st}^{max} was found to be 30% lower, however. This can be accounted for by assuming that T_{1e}/T_{1p} is about twice as large as given by eq. (2.15). Direct measurements of T_{1p} and T_{1e} are being carried out at our laboratory¹. Preliminary results of these measurements confirm that at 3.0 kG T_{1e}/T_{1p} is larger than given by eq. (2.15).

All these measurements were repeated in 2%, 1%, 0.2% and 0.1% CuKS. The results of the measurements are shown in the figs. 4.2 to 4.5. From these figures one sees that all the main features of E_{st} found in the 0.5% CuKS sample were also observed in crystals with a larger or smaller concentration of Cu-ions. Especially E_{st}^{max} proved to be independent of the concentration, as was predicted by the eqs. (4.1) and (2.15).

1.2. $Cu(NH_4)S$, $CuRbS$, $CuCsS$. When the potassium ion in CuKS is replaced by ammonium, rubidium or cesium ions the electron spin-lattice relaxation mechanisms will be different from those found in CuKS². To study the behaviour of E_{st} as a function of Δ , the microwave power and the temperature under these changed circumstances, the experiments were also carried out in 1% $Cu(NH_4)S$, 1% $CuRbS$ and 1% $CuCsS$. In the case of a small microwave power, E_{st} as a function of Δ again showed a structure resembling

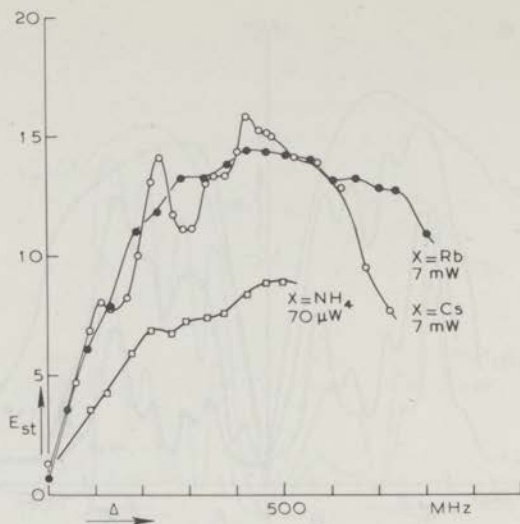


Fig. 4.6. The stationary enhancement E_{st} as a function of Δ in 1% $\text{Cu}(\text{NH}_4)\text{S}$, 1% CuRbS , and 1% CuCsS . The experiments were carried out at about 3.0 kG while T was 1.3 K.

the line shape function $g(\Delta)$. The results in the case of a strongly saturating microwave power P_E and $T = 1.3$ K are shown in fig. 4.6. From this figure can be seen that in the case of 1% $\text{Cu}(\text{NH}_4)\text{S}$ and 1% CuRbS , as in the case of CuKS , the structure which was observed at small microwave power disappeared at a large microwave power.

In the case of 1% CuCsS a second structure in $E_{st}(\Delta)$ as function of Δ appears at very large microwave powers. This structure is shown in fig. 4.6. Contrary to the structure encountered at small microwave powers, it becomes larger, when P_E is increased. This structure furthermore resembles the first derivative of $g(\Delta)$ and not $g(\Delta)$ itself. The explanation of this structure will be discussed in the conclusion of this paper.

From fig. 4.6 can be seen that in the case of 1% CuRbS and 1% CuCsS E_{st}^{max} is again 14 to 15. In the case of 1% $\text{Cu}(\text{NH}_4)\text{S}$, however, a considerable lower enhancement $E_{st}^{max} = 9.0$ was found. According to eq. (4.1) this may be due to the fact that the ratio T_{1e}/T_{1p} for 1% $\text{Cu}(\text{NH}_4)\text{S}$ is much larger than expected from eq. (2.15). To obtain more information about this result, the proton spin-lattice relaxation time is being studied at our laboratory.¹

When the results of the measurements in CuKS , CuRbS , CuCsS and $\text{Cu}(\text{NH}_4)\text{S}$ are compared with each other, it is found that the electron spin-lattice relaxation mechanism has no influence on the behaviour of E_{st} . This is completely in accordance with the predictions of the eqs. (4.1) and (2.15).

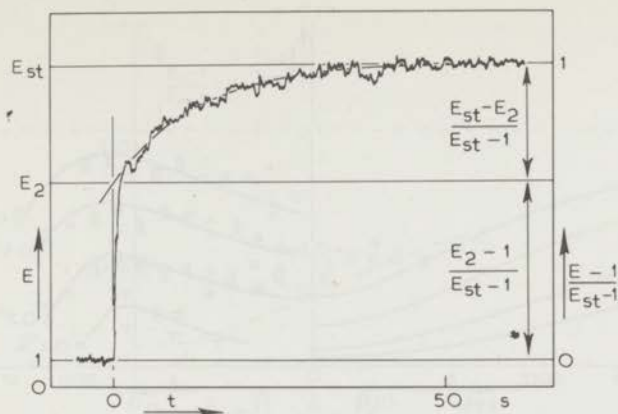


Fig. 4.7. An example of the time behaviour of the enhancement $E(t)$ of the proton signal.

2. *The transient behaviour of the dynamic polarization.* When the microwave field is switched on, the proton spin resonance signal changes from its thermal equilibrium value and finally reaches a stationary enhancement E_{st} . This time behaviour was studied experimentally in all crystals given in table 1 of chapter III. A typical example of such a behaviour is given in fig. 4.7. Within the measuring accuracy the time dependence of the enhancement $E(t)$ can be described by the function:

$$E(t) = E_{st} - (E_{st} - E_2) e^{-t/\tau_1} - (E_2 - 1) e^{-t/\tau_2}, \quad (4.2)$$

where $\tau_1 > \tau_2$. The results of the measurements of τ_1 , τ_2 and the ratio $(E_2 - 1)/(E_{st} - 1)$ will be presented in the following sections.

Theoretically the behaviour given by eq. (4.2) was predicted in chapter II. Furthermore formulae for the behaviour of τ_1 , τ_2 and $(E_2 - 1)/(E_{st} - 1)$ as a function of the saturation parameter s , the microwave frequency and the concentration of Cu-ions were derived. The experimental results will be compared with these theoretical predictions.

2.1 *The coefficient $(E_2 - 1)/(E_{st} - 1)$,* was measured in 1%, 0.5%, 0.2% and 0.1% CuKS as a function of Δ and the microwave power P_E . It was found that in the limit of a strongly saturating microwave field $(E_2 - 1)/(E_{st} - 1)$ is independent of P_E . The measurements of $(E_2 - 1)/(E_{st} - 1)$ as a function of Δ were carried out with such a large value of P_E (10 mW) and at a temperature of 2.0 K. The results of these measurements are given on the right hand side of fig. 4.8.

In the case of strong saturation of the E.S.R. spectrum $(E_2 - 1)/(E_{st} - 1)$ was theoretically predicted in chapter II to be:

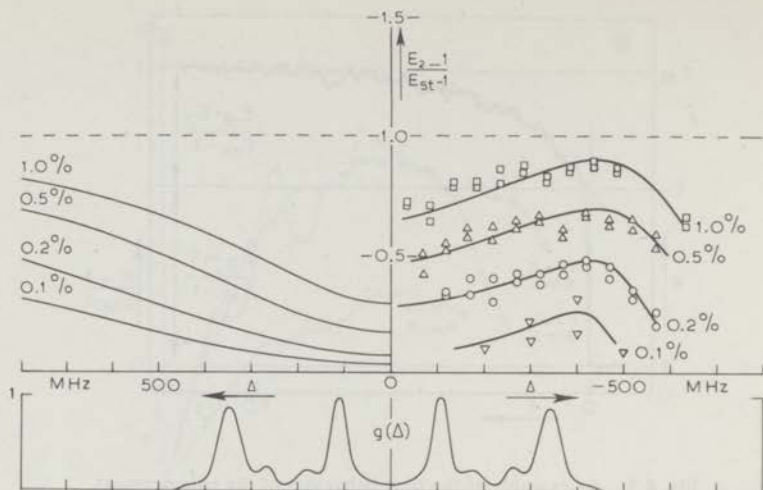


Fig. 4.8. $(E_2-1)/(E_{st}-1)$ as a function of Δ in 1%, 0.5%, 0.2%, and 0.1% CuKS. The experimental curves were obtained at 2.0 K, while P_E was 10 mW.

$$\frac{E_2-1}{E_{st}-1} = \frac{B + \frac{T_{1e}}{T_{1p}}}{B + 1}, \quad (4.3)$$

where:

$$B = \frac{A^2}{\frac{5}{4}A_z^2 + \omega_L^2 + \frac{N_p}{N_e} \omega_p^2}. \quad (4.4)$$

This formula predicts the independence of $(E_2-1)/(E_{st}-1)$ of the saturation parameter s and hence of the microwave power P_E in the limit of strong saturation, which was found experimentally. On the left hand side of fig. 4.8 the theoretical results of $(E_2-1)/(E_{st}-1)$ are plotted. For A_z and ω_L the results of the E.S.R. measurements on the four CuKS samples are used and for T_{1e}/T_{1p} the theoretical relationship given in eq. (2.15) is inserted in eq. (4.3).

We will compare the theoretical and experimental curves in fig. 4.8 on two major features: the value of $(E_2-1)/(E_{st}-1)$ in the limiting case of $\Delta \rightarrow 0$, and secondly the dependence of the ratio $(E_2-1)/(E_{st}-1)$ on Δ . According to the eqs. (4.3) and (4.4), $(E_2-1)/(E_{st}-1)$ is equal to the ratio T_{1e}/T_{1p} in the limit $\Delta \rightarrow 0$. When eq. (2.15) is used for T_{1e}/T_{1p} , theoretical values of $(E_2-1)/(E_{st}-1)$ are found, which are about twice as small, as follows from the experimental results of $(E_2-1)/(E_{st}-1)$. This can be accounted for by

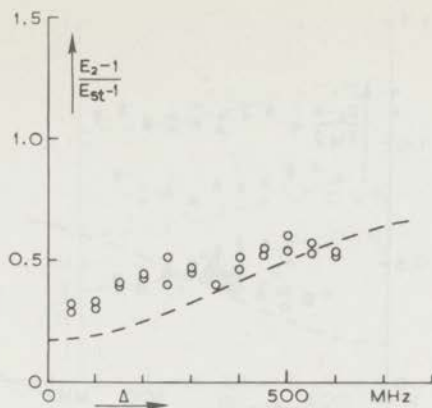


Fig. 4.9. $(E_2-1)/(E_{st}-1)$ as a function of Δ in 1% CuRbS. The experiments were carried out at 1.3 K while P_E was 10 mW.

assuming that T_{1e}/T_{1p} is about twice as large as given by eq. (2.15). This is completely in agreement with the conclusions from the measurements of E_{st}^{max} .

The dependence of $(E_2-1)/(E_{st}-1)$ on $|\Delta|$ is theoretically and experimentally the same in the region $|\Delta| < 400$ MHz. For $|\Delta| > 400$ MHz, however, the experimental curves for $(E_2-1)/(E_{st}-1)$ rapidly decrease contrary to the theoretical predictions. This is due to the fact that for $|\Delta| > 400$ MHz the condition $sg(\Delta) \gg 1$ is no longer satisfied for $P_E = 10$ mW.

The measurements of $(E_2-1)/(E_{st}-1)$ as a function of Δ were repeated in the 0.1% samples of CuRbS and CuCsS at 1.3 K and with a strongly saturating microwave power of 10 mW. The results of these measurements are shown in the figs. 4.9 and 4.10. In these figures theoretical curves obtained from the eqs. (4.3), (4.4) and (2.15) are represented by dotted lines. The deviations between theory and experiment at $\Delta = 0$ can be accounted for in the same way as in CuKS. The dependence on Δ is again adequately described by the theory.

2.2 The time constant τ_1 was, like the coefficient $(E_2-1)/(E_{st}-1)$ measured in 1%, 0.5%, 0.2% and 0.1% CuKS as a function of Δ and P_E . It was found that in the limit of a strongly saturating microwave field, τ_1 , like $(E_2-1)/(E_{st}-1)$ is independent of P_E . The measurements of τ_1 as a function of Δ , presented in fig. 4.11, were carried out with such a large value of P_E (10 mW). The temperature was 2.0 K. In this limit of strong saturation of the E.S.R. spectrum, τ_1 was theoretically derived in chapter II to be given by:

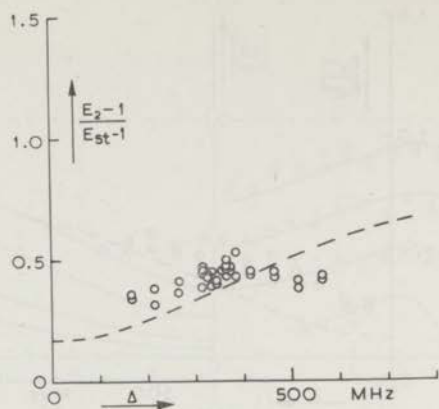


Fig. 4.10. $(E_2-1)/(E_{st}-1)$ as a function of Δ in 1% CuCsS. The experiments were carried out at 1.3 K while P_E was 10 mW.

$$\frac{T_{1e}}{\tau_1} = \frac{B + \frac{T_{1e}}{T_{1p}}}{B + 1},$$

This formula indeed predicts the experimentally found independence of τ_1 on the saturation parameter s and hence the microwave power P_E , when the latter is strongly saturating. It should be noted that in the limit $\Delta \rightarrow 0$, τ_1 is equal to T_{1p} . Theoretical curves for τ_1 are given in fig. 4.11 by means of dotted lines. These curves are obtained as follows. The proton spin-lattice relaxation rate, T_{1p}^{-1} , was determined experimentally by observing the decay of the polarized proton spin resonance signal after switching off the microwave field. The results are given in table 2. These yield the theoretical

Table 2. The experimental values of the proton spin-lattice relaxation rate T_{1p}^{-1} in CuKS at 2.0 K.

c'	T_{1p}^{-1} (sec ⁻¹)
1 %	1.25×10^{-1}
0.5%	1.75×10^{-2}
0.2%	6.20×10^{-3}

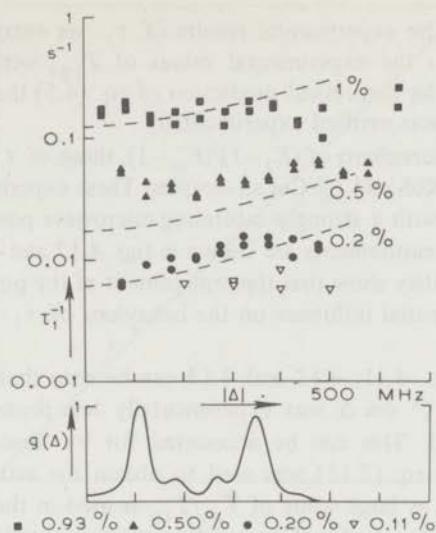


Fig. 4.11. τ_1^{-1} as a function of Δ in 1%, 0.5%, 0.2% and 0.1% CuKS. The experiments were carried out at 2.0 K while P_E was 10 mW.

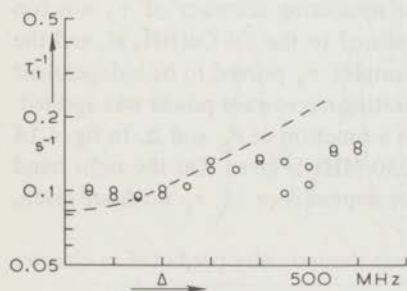


Fig. 4.12. τ_1^{-1} as a function of Δ in 1% CuRbS. The experiments were carried out at 1.3 K while P_E was 10 mW.

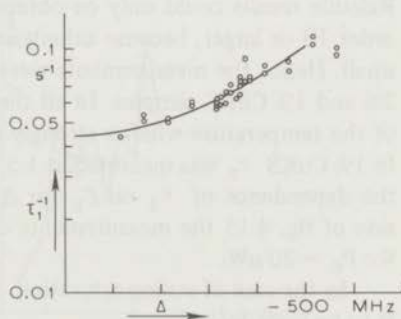


Fig. 4.13. τ_1^{-1} as a function of Δ in 1% CuCsS. The experiments were carried out at 1.3 K while P_E was 10 mW.

values of τ^{-1} in the case of $\Delta = 0$. Then the shape of the theoretical curves is determined with eq. (4.5) by using the theoretical value of T_{1e}/T_{1p} given in eq. (2.15) and the values of A_z and ω_L obtained in E.S.R. experiments on the samples.

Within the measuring accuracy which was about 10% for T_{1p} and τ_1 , the theoretical curves give a good description of the experimental results.

Especially when the experimental results of τ_1 are extrapolated to $\Delta = 0$, they are equal to the experimental values of T_{1p} , within the measuring accuracy. Hence the theoretical prediction of eq. (4.5) that $\tau_1 = T_{1p}$ in the limit of $\Delta = 0$ was verified experimentally.

Like the measurements of $(E_2 - 1)/(E_{st} - 1)$, those of τ_1 were also carried out in the 1% CuRbS and 1% CuCsS samples. These experiments were carried out at 1.3 K and with a strongly saturating microwave power of 10 mW. The results of these measurements are shown in figs. 4.12 and 4.13. Like those of $(E_2 - 1)/(E_{st} - 1)$, they show that the replacement of the potassium ion by Rb^+ or Cs^+ has no essential influence on the behaviour of τ_1 as a function of Δ and T_{1p} .

From the figs. 4.11, 4.12 and 4.13 can be seen that in all samples the dependence of τ_1^{-1} on Δ was experimentally less pronounced than theoretically predicted. This can be accounted for by observing that for the theoretical curves eq. (2.15) was used to obtain the ratio T_{1e}/T_{1p} . When, however, a twice as large value of T_{1e}/T_{1p} is used in the theoretical calculations, the dependence of τ_1^{-1} on Δ will be experimentally and theoretically the same. Hence the measurements of τ_1 , like those of E_{st} and $(E_2 - 1)/(E_{st} - 1)$, show that T_{1e}/T_{1p} is about twice as large as given by eq. (2.15).

2.3 The time constant τ_2 was measured in most crystals of table 1. Reliable results could only be obtained in those crystals where E_2 was of the order 10 or larger, because otherwise the measuring accuracy of τ_2 was too small. Hence the measurements were confined to the 1% Cu(NH₄)S, and the 2% and 1% CuKS samples. In all these samples τ_2 proved to be independent of the temperature when a strongly saturating microwave power was applied. In 1% CuKS τ_2 was measured at 1.5 K as a function of P_E and Δ . In fig. 4.14 the dependence of τ_2 on P_E for $\Delta = 350$ MHz is given. On the right hand side of fig. 4.15 the measurements of the dependence of τ_2 on Δ are given, for $P_E = 20 \mu W$.

In the case of strong saturation τ_2 was theoretically predicted in chapter II to be given by:

$$\frac{1}{\tau_2} = \frac{s.g(\Delta)}{T_{1e}} \cdot (B + 1) = W(\Delta)(B + 1) \quad (4.6)$$

where $W(\Delta)$ is the transition probability induced by the microwave field. According to this equation τ_2 is independent of T_{1e} and hence of the temperature, which is in accordance with the experimental results.

Eq. (4.6) predicts a linear dependence of τ_2^{-1} on the saturation parameters and hence on the microwave power P_E . As can be seen from fig. 4.14 this linear dependence has experimentally been proven to exist. Formula (4.6) furthermore predicts a structure resembling the line shape function $g(\Delta)$

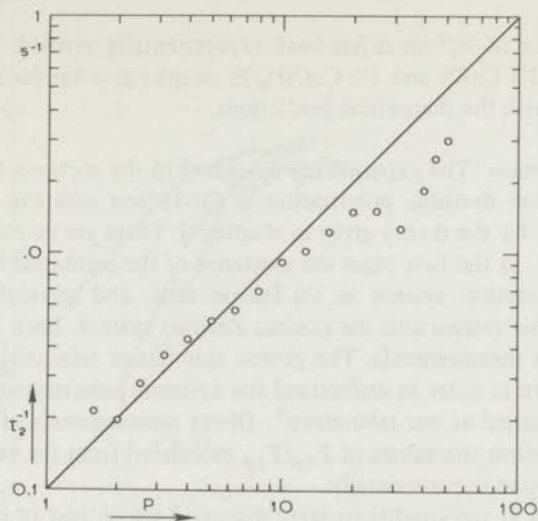


Fig. 4.14. τ_2^{-1} as a function of P_E at $\Delta = 350$ MHz in 1% CuKS. The units of P_E are arbitrary. The experimental data are an average of several measurements.

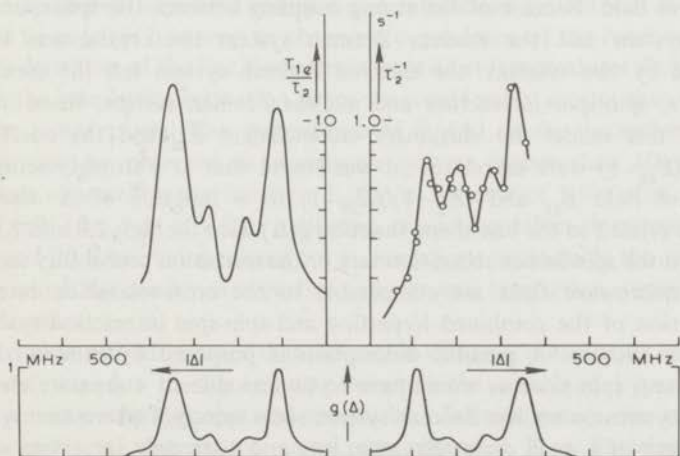


Fig. 4.15. τ_2^{-1} as a function of Δ at $P_E = 20 \mu\text{W}$ in 1% CuKS. The temperature was 1.5 K. The experimental data are an average of several measurements.

in the dependence of τ_2^{-1} on Δ . The predicted structure is given on the left hand side of fig. 4.15. When the experimental and theoretical curves in fig. 4.15 are compared with each other, one sees that the predicted structure in

the dependence of τ_2^{-1} on Δ has been experimentally verified. The measurements in the 2% CuKS and 1% Cu(NH₄)S samples gave similar results, which again agreed with the theoretical predictions.

3, *Conclusion.* The experiments described in the sections 1 and 2 show that the proton dynamic polarization in Cu-Tutton salts can very well be accounted for by the theory given in chapter II. There are two major features in this theory. In the first place the existence of the combined hyperfine and spin-spin interaction system in Cu-Tutton salts, and secondly the strong coupling of this system and the nuclear Zeeman system. Both features were proven by our measurements. The proton spin-lattice relaxation time, which must be known in order to understand the dynamic polarization quantitatively, is being studied at our laboratory¹. Direct measurements of T_{1e} and T_{1p} at 3.0 kG confirm the values of T_{1e}/T_{1p} calculated from the values of E_{st}^{max} which were found experimentally.

In chapter II the conditions were discussed which had to be satisfied to allow the introduction of a combined hyperfine and spin-spin interaction system as a single spin system with one spin temperature. It was pointed out that the introduction of such a system is allowed when the cross relaxation rate between the lines of the E.S.R. spectrum is much larger than the spin-lattice relaxation rate or the transition probability induced by the microwave field. Because of the strong coupling between the spin-spin interaction system and the nuclear Zeeman system the crystal was finally described by two systems: the electron Zeeman system and the combined hyperfine, spin-spin interaction and nuclear Zeeman system. When on the basis of this model the stationary enhancement E_{st} and the coefficient $(E_2 - 1)/(E_{st} - 1)$ were calculated, it was found that at a strongly saturating microwave field E_{st} and $(E_2 - 1)/(E_{st} - 1)$ as a function of Δ show no structure related to the line shape function $g(\Delta)$. (see the figs. 2.2 and 2.6).

When the spin-lattice relaxation rate or the transition probability induced by the microwave field are comparable to the cross relaxation rate, the introduction of the combined hyperfine and spin-spin interaction system is no longer allowed. A possible description is proposed by Provotorov³ in which case 6 spin systems would have to be introduced: 4 separate electron Zeeman systems, a nuclear Zeeman system and a spin-spin interaction system. In the limit of a small cross relaxation rate and a strongly saturating microwave field such a theory would lead to a strong dependence of E_{st} on the line shape function $g(\Delta)$. In this case the function $E_{st}(\Delta)$ would closely resemble the derivative of $g(\Delta)$.

Our experiments were carried out in the temperature region of 1.2 K to 4.2 K and with microwave powers below 10 mW. When the function $E_{st}(\Delta)$ was measured it was found to be independent of the line shape function $g(\Delta)$ at a strongly saturating microwave power of 1 mW. Thus our measurements confirmed that under our experimental conditions the introduction

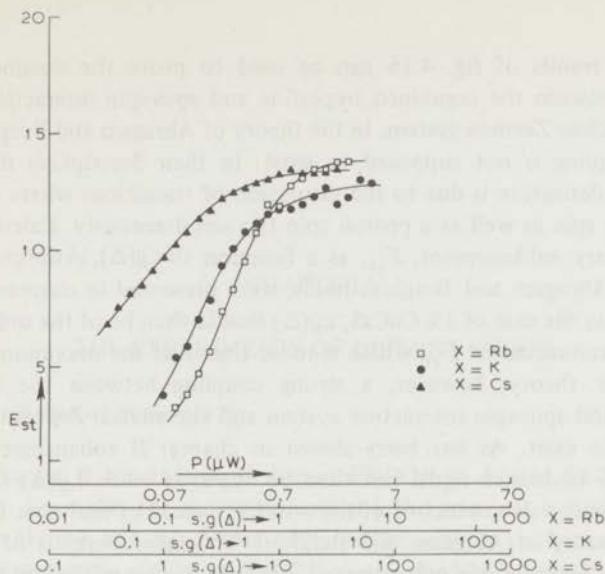


Fig. 4.16. E_{st} as a function of $s.g(\Delta)$ in 0.5% CuKS, 1% CuRbS and 1% CuCsS. The temperature was 1.2 K while Δ was 350 MHz.

of the combined hyperfine and spin-spin interaction system was allowed. It should be possible however, to observe a dependence of the function $E_{st}(\Delta)$ on the derivative of the line shape function $g(\Delta)$ at temperatures above 4.2 K, where the spin-lattice relaxation times are considerably shorter than at liquid Helium temperatures. This dependence of $E_{st}(\Delta)$ on the derivative of $g(\Delta)$ should also be observed at microwave powers higher than 10 mW. The structure observed in the function $E_{st}(\Delta)$ in the case of 1% CuCsS at 1.3 K and 7 mW (fig. 4.6) is a first indication of such an effect. Measurements at 13 K and 20 K are being carried out at our laboratory to study the conditions under which the combined hyperfine and spin-spin interaction system may be introduced.

To obtain another proof that the proton dynamic polarization which was observed was due to the coupling between the combined hyperfine and spin-spin interaction system and the nuclear Zeeman system, the stationary enhancement of the proton signal was measured as a function of the saturation factor $s.g(\Delta)$. The results of these measurements in the case of 0.5% CuKS, 1% CuRbS, and 1% CuCsS are given in fig. 4.16. The experiments were carried out at 1.2 K and for $\Delta = \frac{3}{2}A_z$. The value of $s.g(\Delta)$ in these measurements was obtained by measuring the magnitude of the saturated E.S.R. absorption signal as a function of the microwave power. From fig. 4.16 can be seen that for $s.g(\Delta) = 1$ the enhancement E_{st} is always more than half the maximum value of E_{st} . Similar results were obtained in the other samples of table 1.

These results of fig. 4.16 can be used to prove the assumed strong coupling between the combined hyperfine and spin-spin interaction system and the nuclear Zeeman system. In the theory of Abragam and Borghini⁴ this strong coupling is not supposed to exist. In their description the proton dynamic polarization is due to the saturation of transitions where each time an electron spin as well as a proton spin flip simultaneously. Calculations of the stationary enhancement, E_{st} , as a function of $s.g(\Delta)$, in the case that the theory of Abragam and Borghini holds, were presented in chapter I. It was found that in the case of 1% CuCsS, $s.g(\Delta)$ should then be of the order 10^6 to obtain an enhancement E_{st} which is more than half the maximum value of E_{st} . In our theory, however, a strong coupling between the combined hyperfine and spin-spin interaction system and the nuclear Zeeman system is supposed to exist. As has been shown in chapter II enhancement of the proton spin resonance signal can then be observed when $s.g(\Delta)$ has a considerably lower value, which is of the order 1, instead of the value 10^6 found with the theory of Abragam and Borghini. The measurements of fig. 4.16 show that a considerable enhancement was already observed when $s.g(\Delta)$ was equal to 1. These experimental results again strongly support the theoretical basis of our theory, which presupposes the existence of the strong coupling between the combined hyperfine and spin-spin interaction system and the nuclear Zeeman system.

REFERENCES

1. van den Heuvel, G.M., and Poulis, N.J., Physica to be published.
2. de Vroomen, A.C., Lijphart, E.E., and Poulis, N.J., Physica to be published.
3. Provotorov, B.N., JETP. 42, 882 (1962), Soviet Physics JETP., 15, 611.
4. Abragam, A., and Borghini, M., Progr. in Low Temp. Phys. Vol. IV. p. 384, ed. C.J. Gorter, North-Holland Publ. Co. (A'dam, 1964).

CHAPTER V

THE EXPERIMENTS OF DISTANT ENDOR

Medium Cool, Haskell Wexler (1970)

In chapter II the theory of distant ENDOR in diluted Cu-Tutton salts was given. Formulae for the stationary and the transient behaviour of the increment of the E.S.R. signal were obtained. In order to verify the theoretical results, experiments of distant ENDOR as described in chapter II, section 3.2 and shown in fig. 2.7 were performed in the 1% CuCsS, the 1% CuRbS and the 0.5% CuKS samples of table 1 (chapter III). These experiments were carried out as a function of the microwave power P_E and the N.M.R. coil voltage V_c for several values of Δ . The results of these experiments will be compared with the theoretical formulae of chapter II.

1. 1% CuCsS. Measurements of J_{st} , J_4 , τ_4 , τ_3 , τ_2 and τ_1 were carried out in 1% CuCsS at 1.4 K with the microwave power varying from 0.04 μ W to 4 μ W and an N.M.R. coil voltage V_c of 2.8 V and 5.0 V. Δ was chosen to be 350 MHz, which is at the centre of E.S.R. line no. IV (fig. 5.1). The results of the measurements of J_{st} as a function of s_E are presented in fig. 5.2, while those of J_4 as a function of s_E are presented in fig. 5.3. The experimental values of τ_3 and τ_4 as a function of s_E are given in fig. 5.4, while those of τ_1 and τ_2 as a function of s_E are given in fig. 5.5. In all figures the experimental curves are given as drawn lines. They are obtained by making a best fit through the measuring points.

In order to be able to compare the experimental results described above with the theoretical formulae obtained in chapter II, theoretical curves for the coefficients J_{st} and J_4 and all the time constants are given in the figs. 5.2 to 5.5 by means of dotted lines. These theoretical curves are obtained in exactly the same way as those in the figs. 2.8, 2.10, 2.11 and 2.12. The same values of B and T_{1e}/T_{1p} are also used. s_E is obtained from measurements of the magnitude of the saturated microwave absorption signal as a function of the microwave power. Furthermore T_{1e} was measured directly by de Vroomen and Lijphart with the pulse saturation method.¹ This experiment yielded $T_{1e} = 30$ sec. at 1.4 K. The values of s_N are chosen so as to obtain a best fit of the experimental and theoretical curves for all the measured quantities J_{st} ,

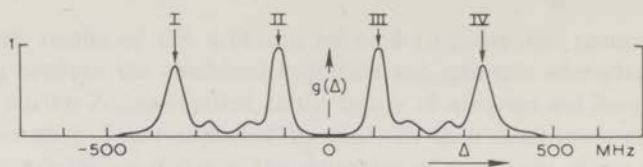


Fig. 5.1. The experimentally determined line shape function $g(\Delta)$ in the case of 1% CuCsS. The crystal was directed with its b-axis parallel to the static magnetic field H_0 .

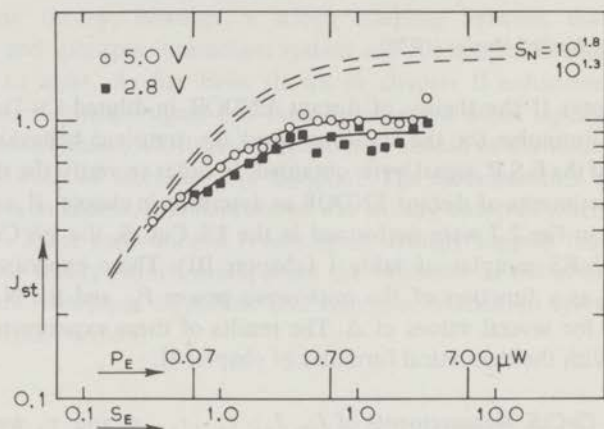


Fig. 5.2. J_{st} as a function of the microwave power P_E for $V_c = 2.8$ V and 5.0 V in 1% CuCsS at $T = 1.4$ K. Theoretical curves for J_{st} are denoted by dotted lines. $s_N = 10^{1.8}$ and $10^{1.3}$ correspond to $V_c = 5.0$ V and 2.8 V respectively.

J_4 , τ_4 and τ_3 simultaneously. This best fit is obtained by choosing $s_N = 10^{1.8}$ for $V_c = 5.0$ V. So: $s_N = 10^{1.3}$ for $V_c = 2.8$ V.

As can be seen from fig. 5.2, the stationary increment J_{st} has experimentally and theoretically the same dependence on s_E and on s_N . However, the experimental values of J_{st} are appreciably smaller than the calculated ones. This can be accounted for by observing that J_{st} is strongly dependent on the ratio T_{1e}/T_{1p} . As has been observed in our experiments of nuclear dynamic polarization in the same crystals (see chapter IV), this ratio has been experimentally found to be twice as large as given by the eq. (2.15). When this larger value of T_{1e}/T_{1p} is introduced into eq. (2.24) the theoretical and experimental curves for J_{st} will coincide within the measuring accuracy.

The experimental results presented in fig. 5.2 can be used to obtain an extra proof of the existence of the strong coupling between the nuclear Zeeman system and the spin-spin interaction system. When this strong

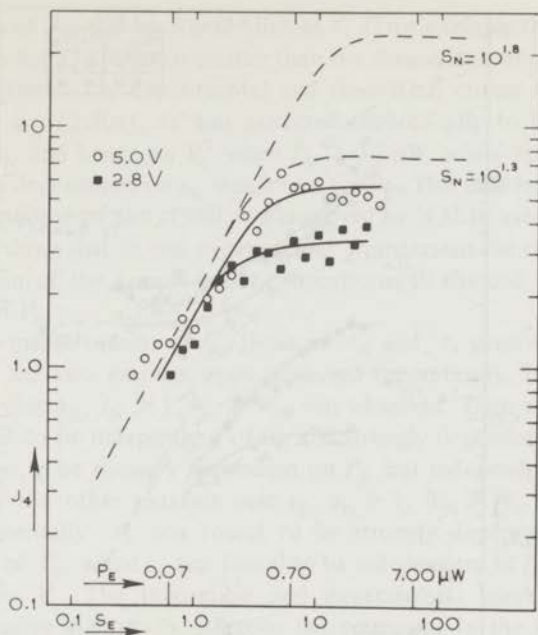


Fig. 5.3. J_4 as a function of the microwave power P_E for $V_C = 2.8$ V and 5.0 V in 1% CuCsS at $T = 1.4$ K. Theoretical curves for J_{st} are denoted by dotted lines. $s_N = 10^{1.8}$ and $10^{1.3}$ correspond to $V_C = 5.0$ V and 2.8 V respectively.

coupling is not supposed to exist, the distant ENDOR effect can only be observed, when 'forbidden' transitions are saturated, where each time an electron, as well as a proton spin flip. In chapter I an estimate was made of the probability of an electron spin to flip owing to such a forbidden transition in the case of a Zinc-Tutton salt containing 1% Cu^{2+} ions. This probability was estimated to be 10^3 times smaller than that of an allowed E.S.R. transition where only an electron spin flips. So s_E would then have to be of the order 10^3 so that the 'forbidden' transitions are 'half saturated' and hence a considerable ENDOR-effect is observed. From fig. 5.2 can be seen, however, that an increment of 0.75 was already obtained for $s_E = 1$, which is more than half the maximum increment obtained. This experimental result again proves the existence of the strong coupling between the nuclear Zeeman system and the spin-spin interaction system.

The experimental curves for J_4 in fig. 5.3 clearly show, that for $P_K 0.7 \mu\text{W}$, J_4 is independent of the microwave power and hence of s_E , but strongly dependent on the rf power and hence on s_N . On the other hand one sees that for $P_E > 0.1 \mu\text{W}$, J_4 is linearly dependent on the microwave power

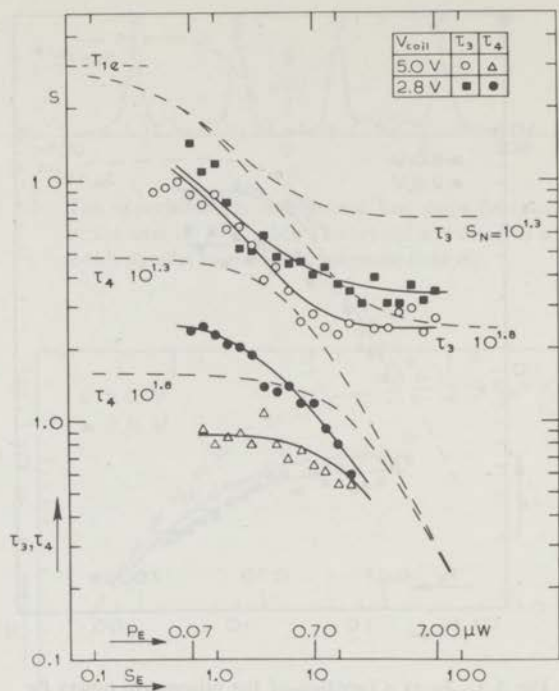


Fig. 5.4. τ_3 and τ_4 as a function of the microwave power P_E for $V_c = 2.8$ V and 5.0 V in 1% CuCsS at $T = 1.4$ K. Theoretical curves for J_{st} are denoted by dotted lines. $s_N = 10^{1.8}$ and $10^{1.3}$ correspond to $V_c = 5.0$ V and 2.8 V respectively.

and hence on s_E , but independent of the rf power and hence of s_N . This is completely in accordance with the theoretical predictions that for $W_o \gg W_N$, J_4 should depend linearly on s_N and be independent of s_E , while for $W_o \ll W_N$, J_4 should be linearly dependent on s_E and independent of s_N . The theoretical and experimental curves in fig. 5.3 disagree with each other in two ways. In the first place the experimental values of J_4 are considerably smaller than those theoretically predicted. This can be explained by taking the response time of the apparatus into account. In an ENDOR experiment as given in fig. 2.7, J_4 is determined by extrapolating the decay, which is described by the time constant τ_3 , backwards in time to the moment t_1 , when the rf field is switched on. This extrapolation is shown in fig. 2.7 together with the resulting value of J_4 . Owing to the response time of the apparatus, which was about 0.15 sec, the ENDOR effect is observed to begin at the moment t'_1 , which is about 0.15 sec. later than the actual moment t_1 that the rf field was switched on. As can be seen from fig. 2.7 at $t'_1 > t_1$ a

smaller value of J_4 will be found than at t_1 . This explains that the experimental values for J_4 are much smaller than the theoretical values. The second difference between the experimental and theoretical curves for J_4 is, that according to eq. (2.30c), J_4 was expected theoretically to be linearly dependent on s_N and hence on V_c^2 when $P_E > 0.7 \mu\text{W}$, while experimentally a much weaker dependence on s_N was found for P_E . This discrepancy is caused by the construction of the rf coil as was proved by N.M.R. saturation experiments. They show that in our experimental arrangement the rf field strength at the position of the sample is not proportional to the coil voltage V_c for large values of V_c .

Like the measurements of J_4 , those of τ_3 and τ_4 presented in fig. 5.4, clearly show the two extreme cases predicted theoretically. For $P_E > 2 \mu\text{W}$ the extreme case $s_E, s_N \gg 1, W_o \gg W_N$ was observed. Then experimentally, τ_3 was found to be independent of P_E and strongly dependent on V_c , while τ_4 was found to be strongly dependent on P_E but independent of V_c . For $P_E < 0.2 \mu\text{W}$ the other extreme case $s_E, s_N \gg 1, W_N \gg W_o$ was observed. Then experimentally τ_3 was found to be strongly dependent on P_E but independent of V_c , while τ_4 was found to be independent of P_E but strongly dependent on V_c . The theoretical and experimental curves in fig. 5.4, however, disagree with each other in two respects. In the first place the experimental values of τ_3 and τ_4 are of the order of 50% shorter than expected theoretically. This can be partly explained in the same way as in the case of J_4 , by taking the response time of the measuring apparatus into account. As can be seen from fig. 2.7 τ_4 and τ_3 are derived from the shape of the curve $J(t)$ by which the final increment J_{st} is reached. As has been pointed out before, owing to the response time of the apparatus, the ENDOR effect is observed to begin at the moment t'_1 which is about 0.15 sec later than the actual moment t_1 that the rf field is switched on. As a result the curve $J(t)$ is distorted in such a way that the observed values of τ_3 and τ_4 will be too short. The second discrepancy between the experimental and theoretical curves for τ_3 and τ_4 is that the dependence of these time constants on V_c^2 is weaker than expected theoretically. This can be explained by the non-linear dependence of the rf field strength H_1 on V_c for large values of V_c so that the actual dependence of τ_3 and τ_4 on s_N is stronger than expected from the dependence of these quantities on V_c^2 .

In fig. 5.5 the experimental values are presented of the time constants τ_1 and τ_2 describing the transient behaviour of the increment $J(t)$ after switching off the rf field. In this figure measurements are also given of the time constants τ'_1 and τ'_2 , describing the transient behaviour of the nuclear dynamic polarization in the same crystal. These latter measurements were also performed at $\Delta = 350 \text{ MHz}$ and $T = 1.4 \text{ K}$. A description of these dynamic polarization measurements has been given in chapter IV. As can be seen from fig. 5.5 the behaviour of τ_1 is exactly equal to the behaviour of τ'_1 , within the measuring accuracy, just as in the case of τ_2 and τ'_2 . This is

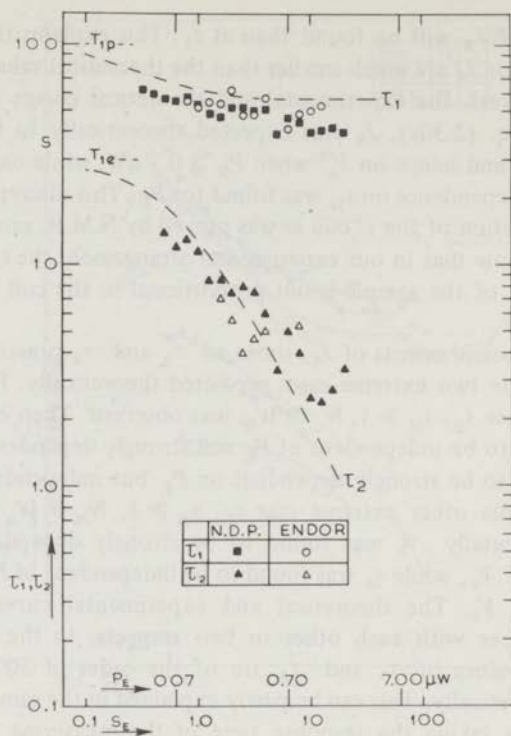


Fig. 5.5. τ_1 and τ_2 measured as a function of s_E in distant ENDOR experiments as well as nuclear dynamic polarization experiments in 1% CuCsS for $\Delta = 350$ MHz at $T = 1.4$ K. Theoretical curves for τ_1 and τ_2 are denoted by dotted lines.

completely in accordance with the theory, because in our distant ENDOR experiments, when the rf field is switched off, and in the case of nuclear dynamic polarization, the same equations (2.13a) and (2.13b) describe the behaviour of the inverse spin temperatures α and β . Hence in both cases the same time constants must be found.

When the experimental results for the time constants τ_1 and τ_2 as a function of P_E are compared with the theoretical curves, one sees that they have the same dependence on P_E . An important feature is that for large microwave power P_E where $s_E \gg 1$, τ_2 becomes linearly dependent on P_E . This has been found experimentally as well as theoretically. An extensive discussion of the behaviour of τ_1 and τ_2 as a function of P_E , Δ and the temperature T , has been given in chapter IV.

To study the influence of the microwave frequency on the distant ENDOR effect, the measurements described above were also performed in the

same sample at the same temperature but at different values of ω : $\Delta = \pm 120$ MHz and $\Delta = -350$ MHz, which is at the centre of the other three resonance lines (I, II and III in fig. 5.1). In all these cases J_{st} was measured with an N.M.R. coil voltage of 5 V and a microwave power so that $s_E = 10$. The resulting values of J_{st} at $\Delta = \pm 120$ MHz were about 10 times smaller than that at $\Delta = 350$ MHz. At $\Delta = -350$ MHz the increment J_{st} was within the measuring accuracy the same as in the case of $\Delta = +350$ MHz. These experimental results agree with the theoretical predictions of eq. (2.24). The coefficient J_4 and the time constants τ_1 , τ_2 , τ_3 and τ_4 were also measured at $\Delta = -350$ MHz. The results of these experiments were in good agreement with the theoretical predictions. At $\Delta = \pm 120$ MHz the transient behaviour of the ENDOR effect could not be studied because the signal to noise ratio of J_{st} was too small.

2. *0.5% CuKS and 1% CuRbS.* When the Cs^+ ions in the samples are replaced by K^+ or Rb^+ , other electron spin-lattice relaxation mechanisms than in the case of CuCsS are encountered.¹ To observe experimentally whether such a change of the electron spin-lattice relaxation mechanism has any influence on the distant ENDOR effect, all the experiments described in the previous sections were repeated in the 0.5% CuKS and the 1% CuCsS samples. The experiments were carried out at 1.3 K and with $\Delta = +350$ MHz at the centre of line IV (fig. 5.1). The stationary increment J_{st} , the coefficient J_4 , and the time constants τ_1 , τ_2 , τ_3 and τ_4 were measured as a function of the microwave power P_E and the N.M.R. coil voltage V_C . The results of the measurements in 0.5% CuKS are presented in the figs. 5.6 to 5.9, while those in 1% CuRbS are presented in the figs. 5.10 to 5.13. Theoretical curves for the parameters J_{st} , J_4 , τ_1 , τ_2 , τ_3 , and τ_4 are obtained in exactly the same way as in the case of 1% CuCsS. Again a good agreement exists between the shape of the theoretical and experimental curves. The differences between the experimental and theoretical curves are the same as those observed in the case of 1% CuCsS. These differences can also be accounted for in the same way. From the results of the measurements it is found that the mechanism of the electron spin-lattice relaxation has no influence on the stationary and the transient behaviour of the distant ENDOR effect.

3. *Conclusion.* The experiments of distant ENDOR described in this paper confirm our description of the spin dynamics of diluted Copper Tutton salts at liquid Helium temperatures.¹ The two major features of this theory were the existence of the combined hyperfine and spin-spin interaction system and furthermore the strong coupling between this system and the nuclear Zeeman system. Experimental proof of both these features was already obtained with our experiments of proton dynamic polarization. Additional proof of the second of these two features was given by our measurements of J_{st} as a function of s_E . Our distant ENDOR experiments

also again proved the existence of the combined hyperfine and spin-spin interaction system, because a large distant ENDOR effect was found at the centre of each of the four E.S.R. lines. In chapter IV it was pointed out that in case no such combined hyperfine and spin-spin interaction system exists, a description should be given with 5 spin systems: four electron Zeeman systems and a combined spin-spin interaction and nuclear Zeeman system. Calculations show that then $J_{st} = 0$ at the centre of each of the four E.S.R. lines, contradicting our measurements.

REFERENCES

1. de Vroomen, A.C., and Lijphart, E.E., *Physica*, to be published.
2. Abragam, A. and Borghini, M., *Progr. in low Temp. Phys.* Vol. IV p. 384, ed. Gorter, North-Holland Publ. Co. (Amsterdam, 1964).

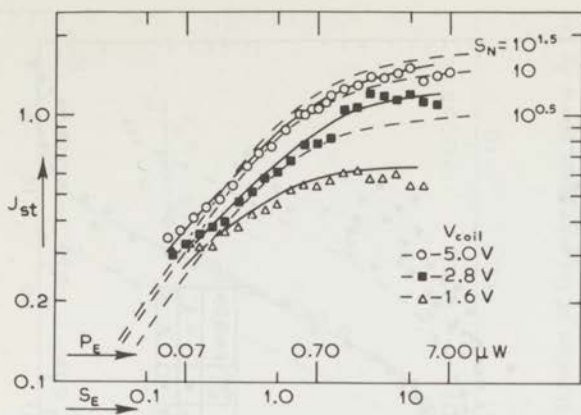


Fig. 5.6. J_{st} as a function of the microwave power P_E for $V_c = 5.0$ V, 2.8 V and 1.6 V in 0.5% CuKs at $T = 1.3$ K. Theoretical curves for J_{st} are denoted by dotted lines. $s_N = 10^{1.5}$, 10 and $10^{0.5}$ correspond to $V_c = 5.0$ V, 2.8 V and 1.6 V respectively.

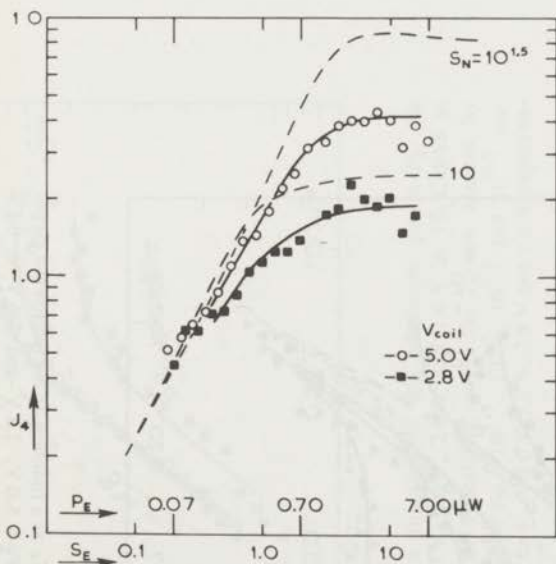


Fig. 5.7. J_4 as a function of the microwave power P_E for $V_c = 5.0$ V and 2.8 V in 0.5% CuKS at $T = 1.3$ K. Theoretical curves for J_4 are denoted by dotted lines. $s_N = 10^{1.5}$ and 10 correspond to $V_c = 5.0$ V and 2.8 V respectively.

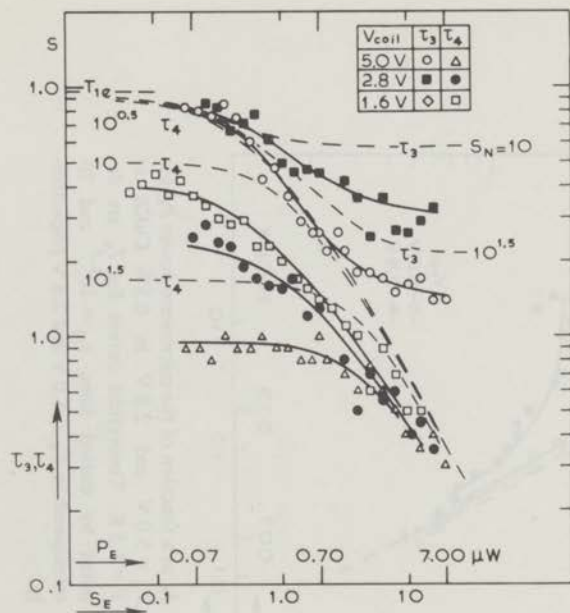


Fig. 5.8. τ_3 and τ_4 as a function of the microwave power P_E for $V_C = 5.0$ V, 2.8 V and 1.6 V in 0.5% CuKS at $T = 1.3$ K. Theoretical curves for τ_3 and τ_4 are denoted by dotted lines. $s_N = 10^{1.5}$, 10 and $10^{0.5}$ correspond to $V_C = 5.0$ V, 2.8 V and 1.6 V respectively.

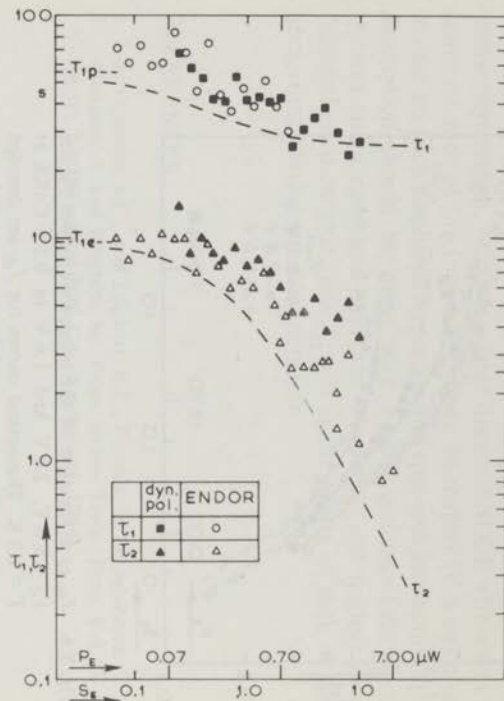


Fig. 5.9. τ_1 and τ_2 measured as a function of s_E in distant ENDOR experiments as well as nuclear dynamic polarization experiments in 0.5% CuKS at $T = 1.3$ K. Theoretical curves for τ_1 and τ_2 are denoted by dotted lines.

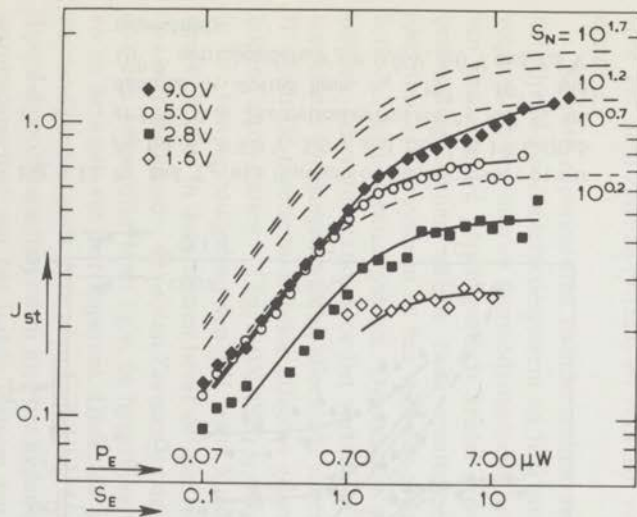


Fig. 5.10. J_{st} as a function of the microwave power P_E for $V_c = 9.0$ V, 5.0 V, 2.8 V and 1.6 V in 1% CuRbS at $T = 1.3$ K. Theoretical curves for J_{st} are denoted by dotted lines. $s_N = 10^{1.7}$, $10^{1.2}$, $10^{0.7}$ and $10^{0.2}$ correspond to $V_c = 9.0$ V, 5.0 V, 2.8 V and 1.6 V respectively.

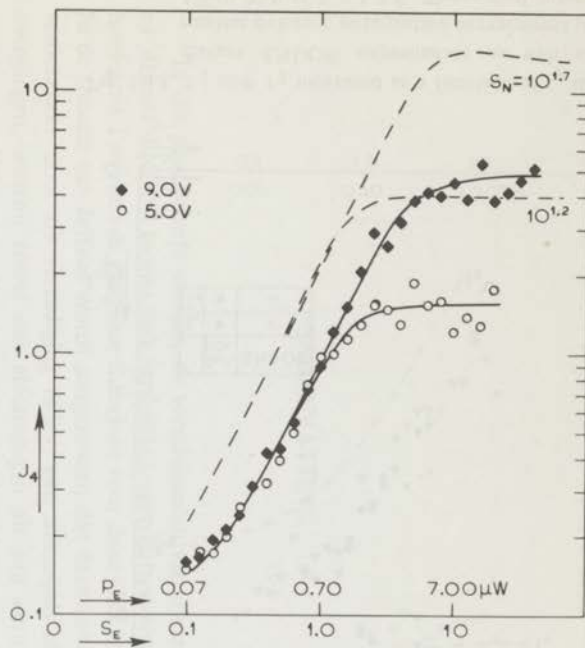


Fig. 5.11. J_4 as a function of the microwave power P_E for $V_c = 9.0$ V and 5.0 V in 1% CuRbS at $T = 1.3$ K. Theoretical curves for J_4 are denoted by dotted lines. $s_N = 10^{1.7}$ and $10^{1.2}$ correspond to $V_c = 9.0$ V and 5.0 V respectively.

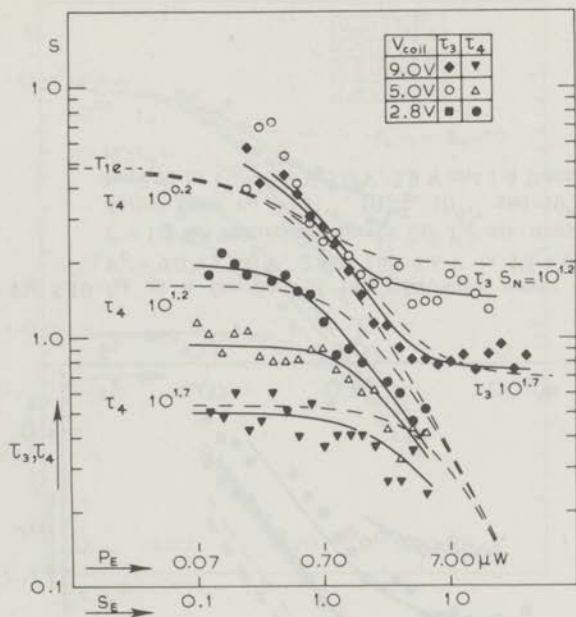


Fig. 5.12. τ_3 and τ_4 as a function of the microwave power P_E for $V_c = 9.0$ V, 5.0 V and 2.8 V in 1% CuRbS at $T = 1.3$ K. Theoretical curves for τ_3 and τ_4 are denoted by dotted lines. $s_N = 10^{1.7}$, $10^{1.2}$ and $10^{0.7}$ correspond to $V_c = 9.0$ V, 5.0 V and 2.8 V respectively.

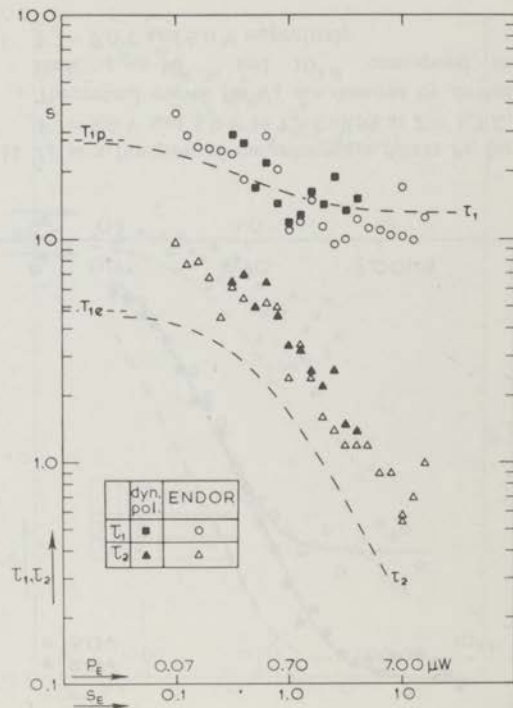


Fig. 5.13. τ_1 and τ_2 measured as a function of s_E in distant ENDOR experiments as well as nuclear dynamic polarization experiments in 1% CuRbS at $T = 1.3$ K. Theoretical curves for τ_1 and τ_2 are denoted by dotted lines.

SAMENVATTING

In dit proefschrift worden de verschijnselen van dynamische polarisatie en 'distant'-ENDOR in met zink verdunde koper-Tutton-zouten behandeld. In hoofdstuk I worden de gangbare theorieën voor deze effecten gerecapituleerd. In de theorie van Jeffries wordt aangenomen dat deze verschijnselen worden veroorzaakt door de verzadiging m.b.v. een microgolfveld van 'verboden' overgangen, waarbij zowel een electronspin als een kernspin tegelijkertijd omklappen. Hij verwaarloosde echter de dipool-dipoolinteractie tussen de electronspins onderling. In de theorie van Abragam en Borghini wordt wel rekening gehouden met deze interactie. Zij gaven een thermodynamische beschrijving van het spinsysteem van een verdund paramagnetisch kristal m.b.v. 3 spintemperaturen: respectievelijk voor het electron-Zeeman-systeem, voor het kern-Zeeman-systeem en voor het electron-dipool-dipoolinteractie-systeem.

Recente experimenten toonden echter een sterke koppeling aan tussen het dipool-dipoolinteractiesysteem en het kern-Zeeman-systeem. Dientengevolge moet een nieuwe thermodynamische beschrijving van het spinsysteem van een verdund paramagnetisch kristal gegeven worden. In deze nieuwe beschrijving komen slechts twee spintemperaturen voor; één voor het electron-Zeeman-systeem en één voor het gecombineerde dipool-dipoolinteractie- en kern-Zeeman-systeem. Dynamische polarisatie en 'distant'-ENDOR worden dan veroorzaakt door het verzadigen m.b.v. een microgolfveld van toegestane overgangen waarbij alleen een electronspin omklapt. In hoofdstuk II wordt de theorie voor beide effecten gegeven in het geval van verdunde koper-Tutton-zouten - $(\text{Zn}, \text{Cu})\text{X}_2(\text{SO}_4)_2 \cdot 6\text{H}_2\text{O}$ met $\text{X} = \text{NH}_4, \text{K}, \text{Rb}, \text{Cs}$ - in het temperatuurgebied van 1 K tot 4 K en magnetische velden van omstreeks 3 kOe. In deze zouten bevat de spin-Hamiltoniaan naast termen t.g.v. de electron-Zeeman-, de proton-Zeeman- en de dipool-dipoolinteractieenergie, ook een belangrijke term t.g.v. de hyperfijninteractie tussen de electronspin en de kernspin van het koperion. Onder de bovengenoemde experimentele omstandigheden geeft deze term aanleiding tot een sterke uitbreiding van het dipool-dipoolinteractiesysteem met het hyperfijninteractiesysteem. Omdat de warmtecapaciteit van het laatste systeem aanzienlijk nauwkeuriger bepaald

kan worden dan die van het dipool-dipoolinteractiesysteem, kunnen in verdunde koper-Tutton-zouten de effecten van dynamische polarisatie en 'distant'-ENDOR kwantitatief zeer goed voorspeld worden.

Om de in hoofdstuk II behandelde theorie experimenteel te verifiëren, werden dynamische polarisatie experimenten uitgevoerd met een N.M.R.-opstelling voor 12 MHz en een 3 cm opstelling om de E.S.R.-lijnen van de koperionen te verzadigen. Eveneens werden 'distant'-ENDOR-experimenten uitgevoerd m.b.v. een 3 cm superheterodyne E.S.R.-opstelling en een 12 MHz zender om de protonspinresonantie te verzadigen. De experimenten werden uitgevoerd bij een statisch magnetisch veld van omstreeks 3 kOe en in het temperatuurgebied van 1.2 K tot 4.2 K. In hoofdstuk III worden de gebruikte opstellingen alsmede de gebruikte preparaten beschreven.

In hoofdstuk IV worden de dynamische polarisatie experimenten behandeld. Zowel het stationaire als het tijdsafhankelijke gedrag van de kernpolarisatie werd bepaald. Het blijkt, dat het tijdsafhankelijke gedrag niet beschreven kan worden m.b.v. één tijdconstante. Binnen de meetnauwkeurigheid is echter een beschrijving met twee tijdconstanten mogelijk, wat in overeenstemming is met de in hoofdstuk II gegeven theorie. De polarisatiefactor en deze tijdconstanten werden als functie van de temperatuur en het vermogen en de frequentie van het microgolfveld bepaald. De meetresultaten blijken in goede overeenstemming te zijn met de in hoofdstuk II behandelde theorie; zij kunnen echter niet verklaard worden met de in hoofdstuk I behandelde oudere theorieën. Deze dynamische polarisatie metingen vormen aldus een nieuw bewijs van het bestaan van de sterke koppeling tussen het dipool-dipoolinteractiesysteem en het kern-Zeeman-systeem. Daarnaast bewijzen zij het bestaan van het hyperfijninteractiesysteem.

In hoofdstuk V worden de 'distant'-ENDOR-metingen behandeld. Ook hier werd zowel het stationaire als het tijdsafhankelijke gedrag van het effect bestudeerd. Evenals in het geval van dynamische polarisatie kan het tijdsafhankelijke gedrag binnen de meetnauwkeurigheid m.b.v. twee tijdconstanten beschreven worden. De meetresultaten zijn in goede overeenstemming zowel met die van de dynamische polarisatie als met de in hoofdstuk II gegeven theorie. Ook deze metingen bevestigen het bestaan van de sterke koppeling tussen het dipool-dipoolinteractiesysteem en het kern-Zeeman-systeem. Eveneens bewijzen zij wederom het bestaan van het hyperfijn interactiesysteem.

Teneinde te voldoen aan het verzoek van de faculteit der Wiskunde en Natuurwetenschappen, volgt hier een kort overzicht van mijn studie.

De eerste beginselen der natuurkunde werden mij op inspirerende wijze bijgebracht door Dr. F.F. Bos op het Rijnlands Lyceum te Wassenaar. Na in 1960 het eindexamen H.B.S.-B aan deze school behaald te hebben, begon ik in hetzelfde jaar mijn studie aan de Rijksuniversiteit te Leiden. Het candidaatsexamen in de wis- en natuurkunde met bijvak sterrenkunde volgde in 1964. Daarna begon ik mijn werkzaamheden op het Kamerlingh Onnes Laboratorium bij de werkgroep voor magnetische resonantie, die onder leiding staat van Prof. Dr. N.J. Poulis. Sinds 1965 heb ik tevens geassisteerd op het natuurkundig practicum. Tot mijn doctoraalexamen in de experimentele natuurkunde, dat ik in 1967 aflegde, verrichte ik experimenten met behulp van ultra- en hypergeluid. De samenwerking met Drs. L.J. Ancher en Drs. M.W. van Tol bij het uitvoeren van deze experimenten is bijzonder waardevol geweest. In 1967 werden de dubbelresonantie experimenten in koper-Tutton-zouten aangevangen. De regelmatige discussies met mijn promotor, Prof. Dr. N.J. Poulis, en de dagelijkse discussies met Dr. T.J.B. Swanenburg, wiens ervaring op het gebied van dubbelresonantieexperimenten een noodzakelijke basis voor het onderzoek vormde, waren bijzonder waardevol. Bij het uitvoeren van de experimenten heb ik achtereenvolgens bijzonder prettig samengewerkt met Drs. H. Hoogstraate, die de ENDOR-apparatuur bouwde, en de heer L.A.H. Scheurs. De regelmatige discussies met Drs. G.M. van den Heuvel waren van grote waarde.

Sinds 1965 ben ik op een korte onderbreking na in dienst geweest van de werkgemeenschap vaste stof van de stichting Fundamenteel Onderzoek der Materie. Aanvankelijk was ik wetenschappelijk assistent, na het doctoraal examen wetenschappelijk medewerker. In 1967 ben ik enige tijd in dienst geweest van de Rijksuniversiteit te Leiden als doctoraal assistent.

Behalve van de wetenschappelijke staf ondervond ik veel steun van het technisch en administratief personeel van het Kamerlingh Onnes Laboratorium. Vooral de medewerking van de heer J. Hoogwerf bij het construeren van de microgolfapparatuur was van groot belang. Ook de zorg van de heren D. de Jong en W. Elbers was onmisbaar voor het welslagen van de metingen.

De uitvoering van dit proefschrift kwam mede tot stand dankzij de heer W.F. Tegelaar, die de tekeningen maakte, en de administratie van het Kamerlingh Onnes Laboratorium, die een groot deel van het typewerk verzorgde, alsmede mejuffrouw A. van Wessel, die de engelse tekst corrigeerde. De medewerking van de North Holland Publishing Company, die gedeelten van de in Physica gepubliceerde tekst ter beschikking stelde, was eveneens bijzonder waardevol.

